J. Fluid Mech. (2006), *vol.* 556, *pp.* 387–419.
doi:10.1017/S0022112006009530 Printed in the United Kingdom

Response of velocity and turbulence in submerged wall jets to abrupt changes from smooth to rough beds and its application to scour downstream of an apron

By SUBHASISH DEY AND ARINDAM SARKAR

Department of Civil Engineering, Indian Institute of Technology, Kharagpur 721302, West Bengal, India

(Received 15 August 2005 and in revised form 8 November 2005)

This paper addresses how the turbulent flow field in submerged wall jets responds to an abrupt change from smooth to rough beds. Experiments were conducted for submerged wall jets having different submergence factors and jet Froude numbers. The bed configurations investigated consisted of different combinations of the lengths of smooth beds and the roughness of rough beds. The vertical profiles of time-averaged velocity components, turbulence intensity components and Reynolds stress were detected by an acoustic Doppler velocimeter at different streamwise distances; and the horizontal distributions of bed shear stress were estimated from the Reynolds stress profiles. The flow field displays the decay of jet velocity due to abrupt changes from smooth to rough beds. The boundary layer grows more quickly with increase in roughness of rough beds. The change in bed roughness induces an increased depression of the free surface over the smooth bed. The Reynolds and bed shear stresses are also computed by solving the Navier–Stokes equations. The response of the turbulent flow characteristics of submerged wall jets to abrupt changes from smooth to rough beds is analysed from the point of view of similarity, growth of the length scale, and decay of the velocity and turbulence characteristics scales. The significant observation is that the flow in the fully developed zone is plausibly self-preserving on both smooth and rough beds. Also, the use of a common length scale makes it possible to collapse all the flow data onto a single band; and there is a gradual variation of flow at the junction of the smooth and rough beds.

The equilibrium scour profiles downstream of a smooth apron due to submerged wall jets are computed from the threshold condition of the sediment particles on the scoured bed. Use of the modified bed shear stress for the downstream variation of scoured bed permits the computation of the equilibrium scour profiles. The time-variation of maximum scour depth is computed from the bed shear stress with a modification for the time dependence. The agreement between the results obtained from the model and the experimental data is satisfactory.

1. Introduction

When a submerged wall jet passes over a bed with an abrupt change in bed roughness, the characteristics of velocity and turbulence are different from those of the corresponding jet over a homogenous rough bed as a result of the roughness discontinuity. Most of the prior investigations on an abrupt change in bed roughness were on uniform flow in closed conduits or open channels (Townsend 1966; Antonia &

Luxton 1971; Schofield 1981; Nezu & Tominaga 1994; Chen & Chiew 2003). However, little attention has so far been paid to the flow characteristics of submerged wall jets on abrupt changes of bed roughness. The problem is not only important from the fundamental view point, but also in the context of its potential application to determine the scour downstream of an apron due to submerged wall jets. To be more explicit, when a submerged wall jet flows on a horizontal bed having an abrupt change in bed roughness, e.g. a smooth rigid bed (say an apron) followed by a rough sediment bed, it leads to a local scour downstream of the rigid apron.

Therefore, first the present study (experimental and theoretical) addresses how the flow and turbulence characteristics of horizontal submerged wall jets respond to an abrupt change from smooth to rough beds (§§ 3, 4, 5 and 6). Secondly, based on these findings, it focuses on a methodology to determine the scour profiles and the time-variation of scour of sediment beds downstream of an apron due to submerged jets issuing from a sluice opening (§ 7). Experiments were carried out on the scour downstream of an apron to validate the analytical scour model.

When summarizing the previous studies along the lines of the present study, it is important to mention that Long, Steffler & Rajaratnam (1990) and Wu & Rajaratnam (1995) viewed the submerged wall jets as transitional phenomena between wall jets and free jumps. Therefore, a brief outline of the important studies on wall jets, free jumps and submerged wall jets are given in addition to those on scour downstream of an apron due submerged wall jets.

1.1. *Studies on wall jets, free jumps and submerged wall jets*

Based on the boundary layer theory, Glauert (1956) analysed the wall jet on a horizontal bed. Schwarz & Cosart (1961) estimated the bed shear and Reynolds stresses in a turbulent wall jet by solving the equations of motion for a steady turbulent flow. Rajaratnam (1967) measured the velocity and bed shear stress for plane turbulent wall jets on artificial rough beds, using Pitot and Preston tubes, respectively. Ead & Rajaratnam (2002) found that for low tailwater depths, the momentum flux of the flow in the wall jets decays appreciably with the distance due to the entrainment of reversed flow. Tachie, Balachandar & Bergstrom (2004) measured the flow characteristics of a plane turbulent wall jet and reported that the bed roughness is the cause of an increase the inner-layer thickness, but the jet half-width is nearly independent of bed roughness.

Rajaratnam (1965) analysed the free (hydraulic) jump as a two-dimensional wall jet. The mean velocity profiles in the outer layer of a free jump were found to be self-preserving when the velocity and length scales were used as issuing jet velocity and jet thickness, respectively. Rajaratnam (1968) observed the free jumps on rough beds to be considerably shorter than those on smooth bed. Hughes & Flack (1984) investigated the physical characteristics of the free jump on rough beds. They reported that the bed roughness is the cause of reduction of the tailwater depth and the length of the jump. Long *et al.* (1990) measured the velocity, turbulence intensity and Reynolds stress with a laser Doppler anemometer to study the flow characteristics of submerged wall jets on smooth bed. They found some degree of self-preserving flow characteristics in the fully developed zone. Wu & Rajaratnam (1995) made a comparative study amongst free jumps, submerged jumps and wall jets with the conclusion that the submerged wall jet is the transition between the wall jet and the free jump.

1.2. *Studies on scour downstream of an apron due to submerged wall jets*

Local scour downstream of an apron due to submerged wall jets was studied by Chatterjee & Ghosh (1980), Hassan & Narayanan (1985), Dey & Westrich (2003)

and Hopfinger *et al.* (2004). Chatterjee & Ghosh (1980) measured the velocity profiles in submerged wall jets as they develop over the apron followed by the scour hole. Hassan & Narayanan (1985) studied the flow characteristics and the similarity of scour profiles downstream of an apron due to a submerged wall jet. They proposed a semi-empirical theory based on the characteristic mean velocity in the scour hole to predict the time-variation of scour depth. Dey & Westrich (2003) measured the variation of the boundary layer thickness from the measured velocity profiles at different streamwise locations (over the apron and within the scoured bed of cohesive sediments). They developed empirical relationships for the variation of the boundary layer thickness and obtained an expression for bed shear stress from the solution of the von Kármán momentum integral equation. Recently, Hopfinger *et al.* (2004) described the scour process downstream of a short apron due to submerged jets and proposed a method to predict the time-variation of scour depth using the findings of Hogg, Huppert & Dade (1997), who put forward a model to compute the scour profiles due to horizontal turbulent wall jets without an apron.

2. Experimental setup and measurement techniques

Experiments were carried out in an open channel flume with fixed and mobile beds. In the fixed-bed experiments, submerged wall jets were tested on a horizontal rigid bed with abrupt changes from smooth to rough; and in the mobile-bed experiments, tests were performed on scour of non-cohesive sediment beds downstream of a rigid apron.

2.1. *Fixed bed experiments*

Figure 1(*a*) shows schematic view of the experimental setup for the fixed bed experiments to study submerged wall jets over abrupt changes from smooth to rough beds. The flume was 0.6 m wide, 0.71 m deep and 10 m long. A sediment recess of 0.3 m deep and 2 m long having the same width as the flume was constructed. The sidewalls of the flume were made of transparent glass to facilitate optical access. A Perspex vertical sluice gate, which had a streamlined lip to produce a supercritical stream with a thickness equal to the gate opening, was fitted over the smooth apron. Different sluice gate openings b (=10 mm, 12.5 mm and 15 mm) were achieved by adjusting the gate vertically; and the gate was moved horizontally to vary the length L (= 0.4 m, 0.5 m and 0.55 m) of the smooth apron. In order to make a rough bed, the sediment in the recess was levelled in such a way so that the crest of the roughness (that is the top of sediment particles) was aligned with the surface of the apron. A synthetic resin mixed with water was sprayed uniformly over the levelled sediment bed to stabilize it. When the sediment was sufficiently impregnated with the resin it was left to set for a period of 24 h. Having dried further for up to 48 h, the rough bed was rock-hard. Different rough beds were created using uniform sediments of median diameters $d_{50} = 0.8$ mm, 1.86 mm and 3 mm. The equivalent sand roughness ε, determined from the velocity profiles of uniform flows setting over rough beds formed by the same sediments in a different flume, was approximately equal to d_{50}. The water discharge at the inlet, controlled by an inlet valve, was measured by a calibrated V-notch weir. An adjustable tailgate downstream of the flume controlled the tailwater depth. The free-surface profile was measured by a point gauge. A total of thirty-nine experiments were run for submerged wall jets over abrupt changes of bed roughness; thirteen experiments for each rough bed. Table 1 furnishes the important experimental parameters of different runs for various combinations of

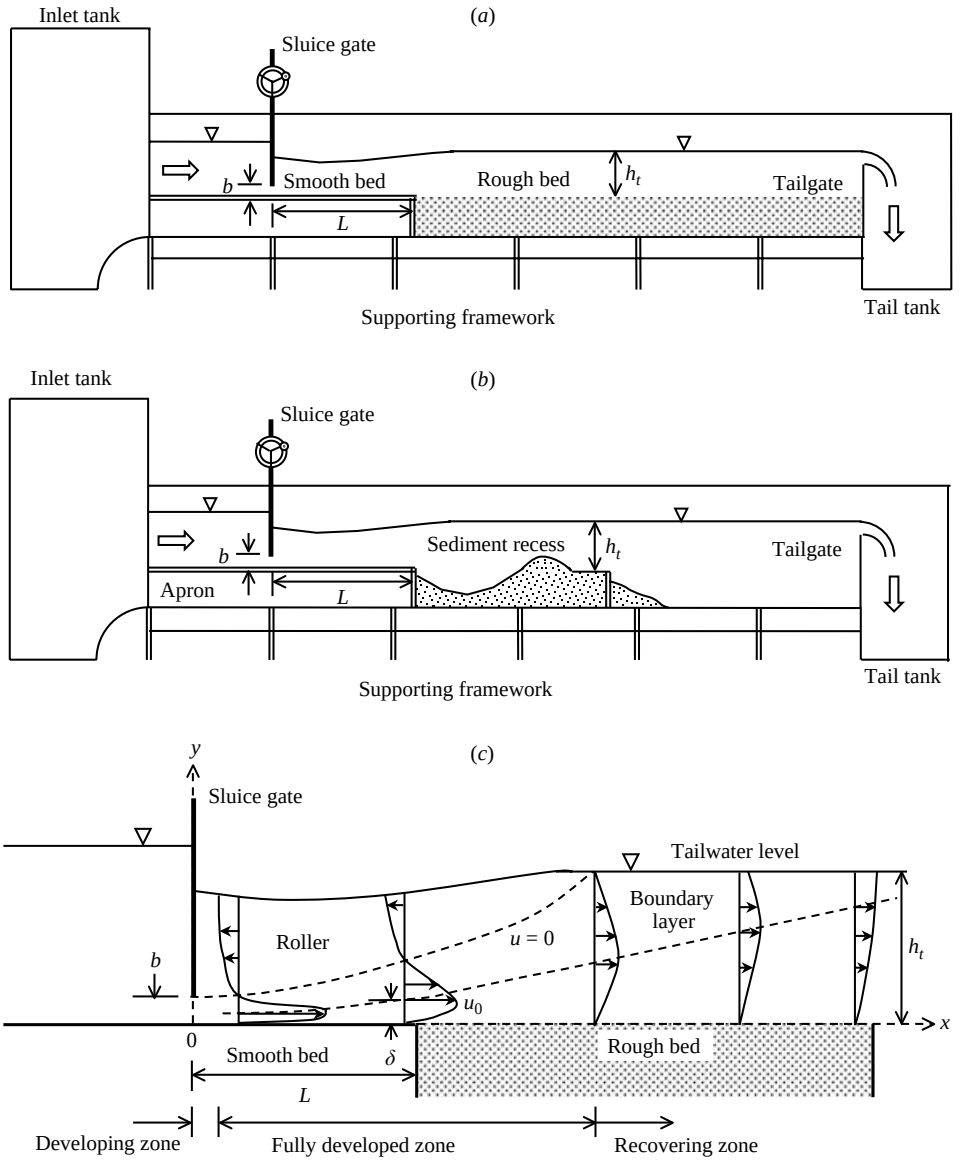

FIGURE 1. (*a*) Schematic diagram of the fixed bed experimental setup for a submerged wall jet on a rigid bed with abrupt changes of bed roughness, (*b*) schematic diagram of mobile bed experimental setup for scour downstream of an apron due to a submerged jet issuing from a sluice opening and (*c*) diagram showing the flow zones in a submerged wall jet.

smooth and rough beds. Here, submergence ratio S and jet Froude number F are defined $(h_t - h_j)/h_j$ and $U/(gb)^{0.5}$, respectively, where h_t is the tailwater depth, h_j is the corresponding tailwater depth of a free jump $[=0.5b(\sqrt{1+8F^2}-1)]$, U is the issuing jet velocity and g is the gravitational acceleration.

Velocity and turbulence profiles were measured by a SonTek 5 cm downlooking acoustic Doppler velocimeter (ADV), which had a sampling rate and volume of 50 Hz and 0.09 cm^3, respectively. A spike removal algorithm filtered the output data from the ADV. The ADV measurements were taken in the vertical plane of symmetry

L (m)	b (mm)	U (m s^{-1})	h_t (m)	h_j (m)	S	F
0.55	10	1.525	0.128	0.064	0.99	4.87
0.5	10	1.49	0.123	0.062	0.96	4.75
0.5	10	1.31	0.114	0.054	1.09	4.18
0.5	12.5	1.435	0.141	0.066	1.12	4.09
0.5	12.5	1.35	0.128	0.062	1.05	3.85
0.5	15	1.21	0.163	0.060	1.72	3.15
0.5	15	0.99	0.136	0.048	1.85	2.58
0.4	10	1.49	0.123	0.062	0.96	4.75
0.4	10	1.31	0.114	0.054	1.09	4.18
0.4	12.5	1.435	0.141	0.066	1.12	4.09
0.4	12.5	1.35	0.128	0.062	1.05	3.85
0.4	15	1.21	0.163	0.060	1.72	3.15
0.4	15	0.99	0.136	0.048	1.85	2.58

TABLE 1. Parameters for different experimental runs. Note: Experiments were done for different bed roughness $\varepsilon = 0.8$ mm, 1.86 mm and 3 mm.

(VPS) along vertical lines at different streamwise distances. In order to check the two-dimensionality of the flow, the ADV measurements were also taken in other vertical planes at a transverse distance of 10 cm from either side of the VPS. The velocity profiles in these planes revealed that in the central part of the flume, the flow was reasonably two-dimensional.

2.2. *Mobile-bed experiments*

Figure 1(*b*) shows a schematic view of the experimental setup for the mobile bed experiments to study the scour downstream of an apron due to submerged jets issuing from a sluice opening. The experiments were conducted in the same flume described in § 2.1 having a similar setup, but the sediment in the recess remained loose (not stabilized). In order to avoid the undesirable erosion of the sediment bed due to sheet flow, the flume was initially filled with water from the downstream side of the sediment recess. Once the water level reached the desired depth, the experiments were run by adjusting the discharge to the desired value. In the initial stage, the scour hole geometry started changing rapidly with time. The scour profiles at regular interval of time were traced on a transparent Perspex sheet attached to the outside glass wall. The Perspex sheet had square grids of size 1 cm × 1 cm to facilitate reproduction of scour profiles. Equilibrium scour holes were obtained after 10 h to 12 h. A number of intermediate and equilibrium scour holes were stabilized for the ADV measurements to determine the bed shear stresses from the Reynolds stress profiles within the scour holes.

3. Flow field in submerged wall jets on abrupt changes from smooth to rough beds

Figure 1(*c*) illustrates the different flow zones (developing, fully developed and recovering zones) of a submerged wall jet, and the coordinate system. The time-averaged velocity components (u, v) correspond to (x, y). The vertical profiles of velocity and turbulence characteristics are represented in a non-dimensional $(\hat{x}, \hat{y})$-plane at different non-dimensional streamwise distances $\hat{x}$, where $\hat{x} = x/b$ and $\hat{y} = y/b$. The lowest vertical and horizontal resolutions of the ADV measurements were 0.2 cm

and 2 cm, respectively. In the following sections, figures 2–8 representing different aspects of the flow field do not show all the experimental data at the lowest resolution so as to avoid overlapping of profiles and data plots. In figures 2–8, the profiles of velocity and turbulence characteristics on rough beds are magnified using representative scales of the velocity and turbulence different from those on smooth beds. Smooth-bed data are shown by open symbols, and rough-bed data by filled symbols. In order to have a comparative study on the influence of the downstream rough beds on the flow field, each of figures 2–8 shows three different runs for three rough beds having identical length of smooth bed L, jet velocity U and sluice opening b. However, other runs are used to analyse the flow characteristics (figures 11–17).

3.1. *Velocity profiles*

The vertical profiles of non-dimensional time-averaged horizontal velocity component $\hat{u}(=u/U)$ at different streamwise distances $\hat{x}$, in submerged wall jets on a rigid bed with abrupt changes from smooth to rough beds, are shown in figure 2. The horizontal velocity component $\hat{u}$ reveals the characteristics of the submerged wall jet issuing from the sluice over different flow zones, namely developing, fully developed and recovering zones. The developing zone of the jet was close to the sluice opening. Hence, it was not always possible to detect the complete flow field in the developing zone due to the ADV limitation. In figure 2, the upper and lower lines represent the loci of $\hat{u} = 0$ and the boundary layer in the submerged wall jets. It is observed that the length of the fully developed zone, where $\hat{u}$ is reversal, decreases with increase in bed roughness ε for the same length L of the smooth bed. The positions of the maximum $\hat{u}$ in the individual profiles, show that the boundary layer grows more quickly in the presence of the rough beds in general, and with increase in roughness in particular. This phenomenon is also obvious from the free-surface profiles. The most important feature to be noticed is the depression of the free-surface elevation and the variation of free-surface curvature in the developing and fully developed zones on the smooth bed with increase in bed roughness ε. This implies that the effect of the roughness ε of a rough bed on the flow over a smooth bed is prominent. The reversal mode of $\hat{u}$, in the fully developed zone, signifies an apparent surface roller (swirl flow), while in the recovering zone, the flow is nearly horizontal.

The vertical profiles of non-dimensional time-averaged vertical velocity component $\hat{v}(= v/U)$ at different $\hat{x}$, in submerged wall jets on a rigid bed with abrupt changes from smooth to rough beds, are presented in figure 3. It is shown that above the bed the direction of $\hat{v}$, being downward on the smooth bed, changes from downward to upward at the junction of the smooth and rough beds. This is due to the roller flow above the expanding jet. From an observation of the flow fields, it is revealed that the upward motion of the flow increases with increase in roughness ε of the rough beds. Therefore, the frictional resistance exerted by the bed roughness on the submerged wall jet is distinguishable in the fully developed zone. In the profiles of $\hat{v}$ on the smooth bed, it is evident that the effect of the bed roughness on the submerged wall jet reduces the downward flow (see figure 3*c*).

Figure 4 depicts the non-dimensional velocity vectors in submerged wall jets on a rigid bed with abrupt changes from smooth to rough beds. The magnitude and direction of velocity vectors are given by $(\hat{u}^2 + \hat{v}^2)^{0.5}$ and arc $\tan(\hat{v}/\hat{u})$, respectively. The characteristics of the decay of jet velocity including a roller flow in the fully developed zone are obvious. Importantly, no noticeable discontinuity in the velocity distributions is observed due to abrupt changes of bed roughness. The behaviour is different from that observed in closed-conduit flows, where an overshooting property

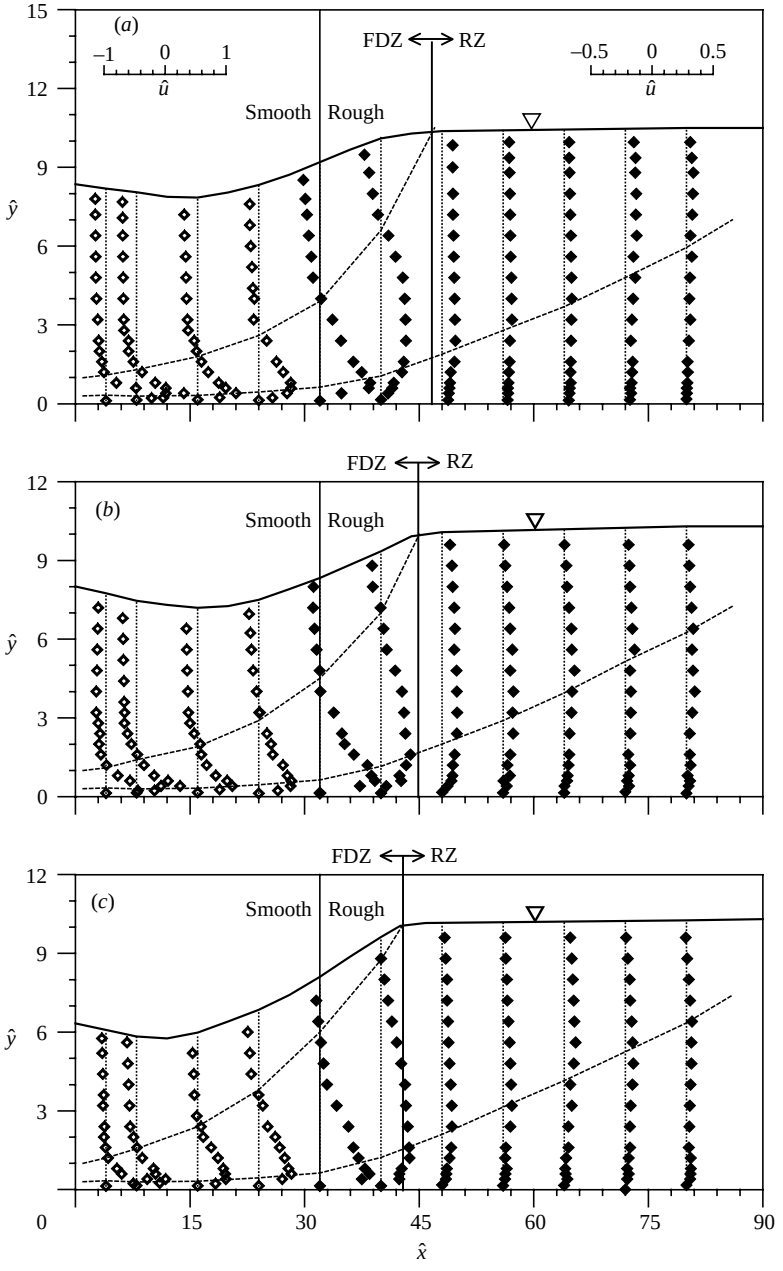

FIGURE 2. Vertical profiles of $\hat{u}$ for $U = 1.435\,\mathrm{m\,s^{-1}}$, $L = 0.4\,\mathrm{m}$ and $b = 12.5\,\mathrm{mm}$: (*a*) $\varepsilon = 0.8\,\mathrm{mm}$, (*b*) $\varepsilon = 1.86\,\mathrm{mm}$ and (*c*) $\varepsilon = 3\,\mathrm{mm}$ (FDZ and RZ refer to the fully developed and recovering zones, respectively).

was reported (Antonia & Luxton 1971). A possible reason for this difference is that when an open channel flow is subjected to an abrupt change of bed roughness, the flow field adjusts gradually through the change of free-surface profile (Chen & Chiew 2003). Also, there was no step change due to roughness in the present case, which might be another reason.

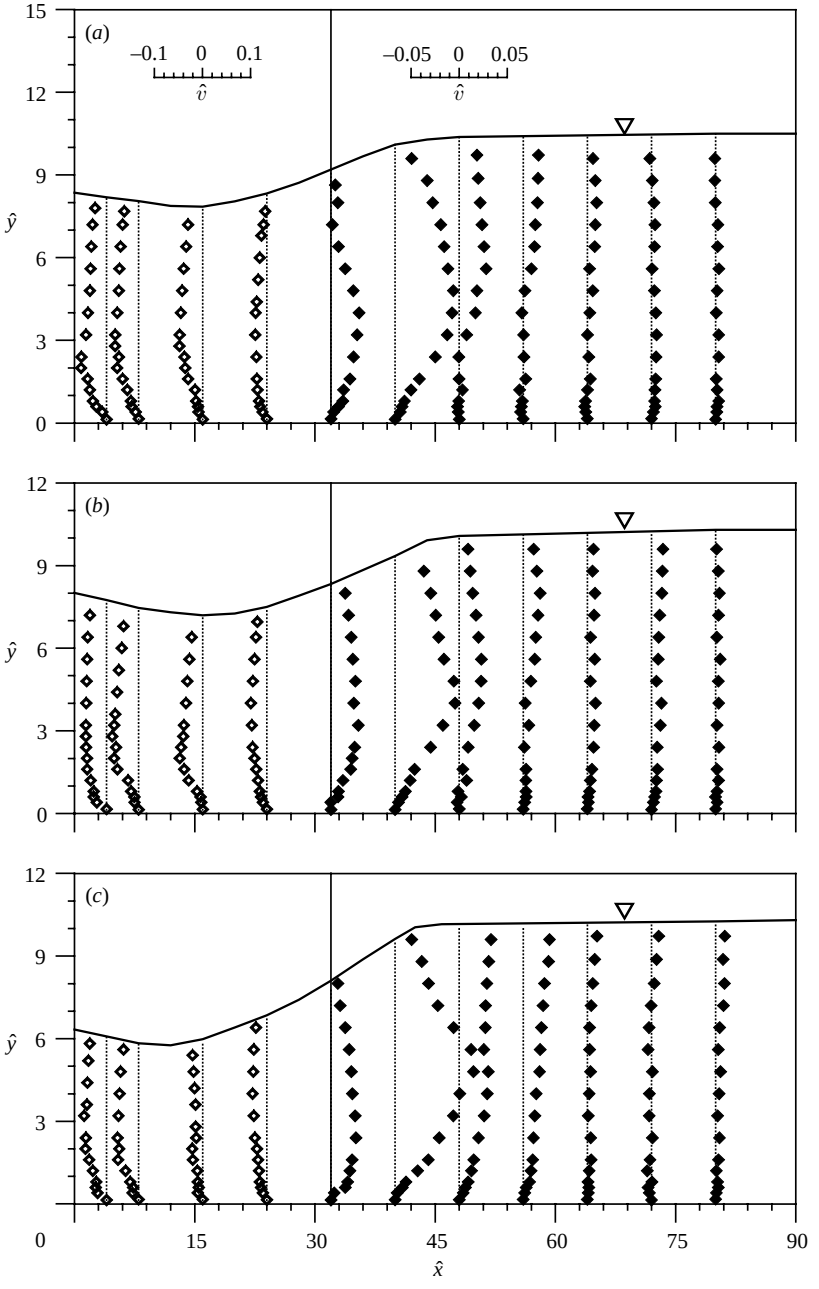

FIGURE 3. Vertical profiles of $\hat{v}$ for $U = 1.435\,\mathrm{m\,s^{-1}}$, $L = 0.4\,\mathrm{m}$ and $b = 12.5\,\mathrm{mm}$: (*a*) $\varepsilon = 0.8\,\mathrm{mm}$, (*b*) $\varepsilon = 1.86\,\mathrm{mm}$ and (*c*) $\varepsilon = 3\,\mathrm{mm}$.

3.2. *Turbulence intensity profiles*

The vertical profiles of the non-dimensional horizontal turbulence intensity component $u^+ (= (\overline{u'u'})^{0.5}/U$, where u' is the fluctuation of u) at different $\hat{x}$, in submerged wall jets on a rigid bed with abrupt changes from smooth to rough beds, are plotted in figure 5. Pronounced bulges in the profiles of u^+ on the smooth bed are apparent as a result of reversed flow. On the rough beds, the profiles of u^+ have continuity

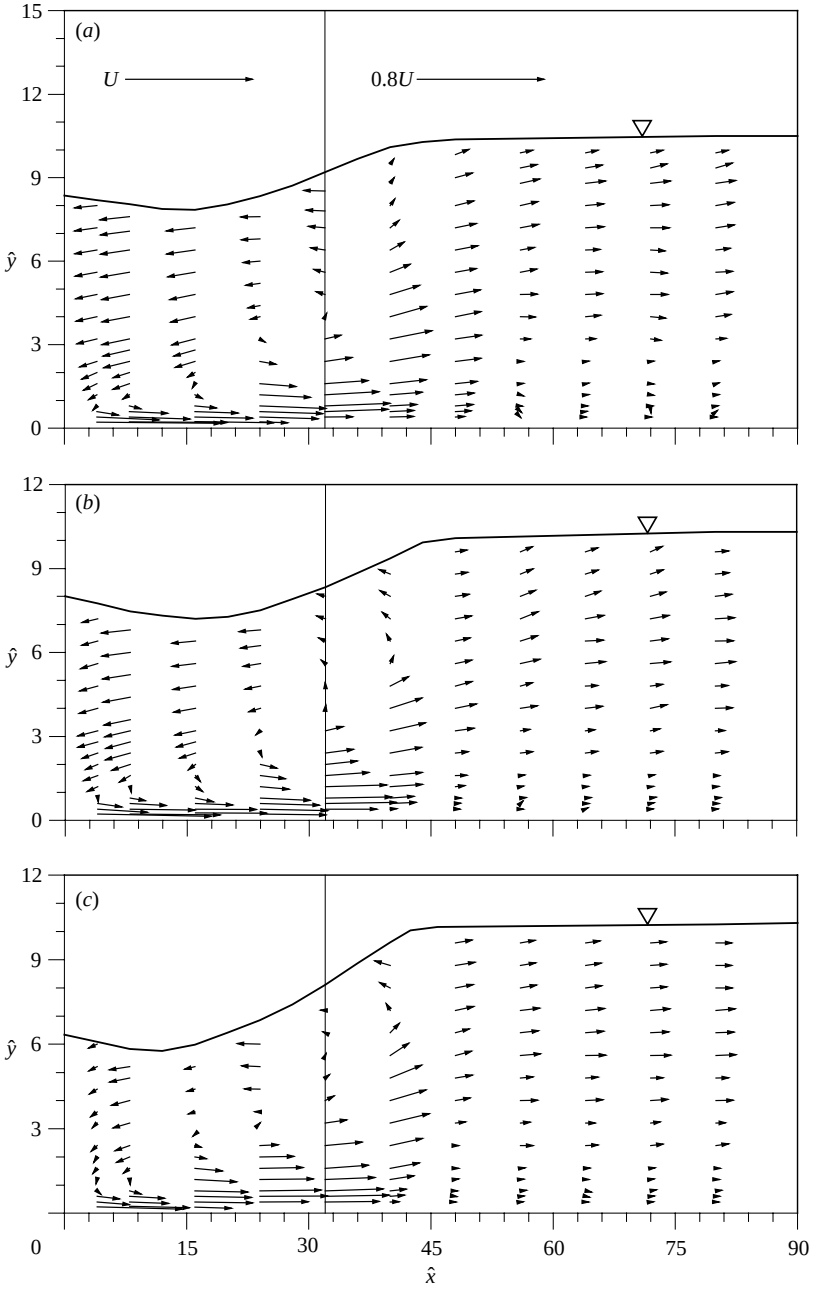

FIGURE 4. Non-dimensional velocity vectors for $U = 1.435\,\mathrm{m\,s^{-1}}$, $L = 0.4\,\mathrm{m}$ and $b = 12.5\,\mathrm{mm}$: (*a*) $\varepsilon = 0.8\,\mathrm{mm}$, (*b*) $\varepsilon = 1.86\,\mathrm{mm}$ and (*c*) $\varepsilon = 3\,\mathrm{mm}$.

(that is the change is gradual) with those of smooth bed, in the fully developed zone. On the other hand, in the recovering zone, u^+ increases with increase in vertical distance $\hat{y}$ over a short distance, then becoming almost constant over the entire zone. In the fully developed zone, u^+ increases with increase in $\hat{y}$, becoming maximum at approximately $\hat{y} = 0.5$–0.6, and then decreases gradually with increase in $\hat{y}$. The local maximum value of u^+ of a vertical profile increases initially with increase in

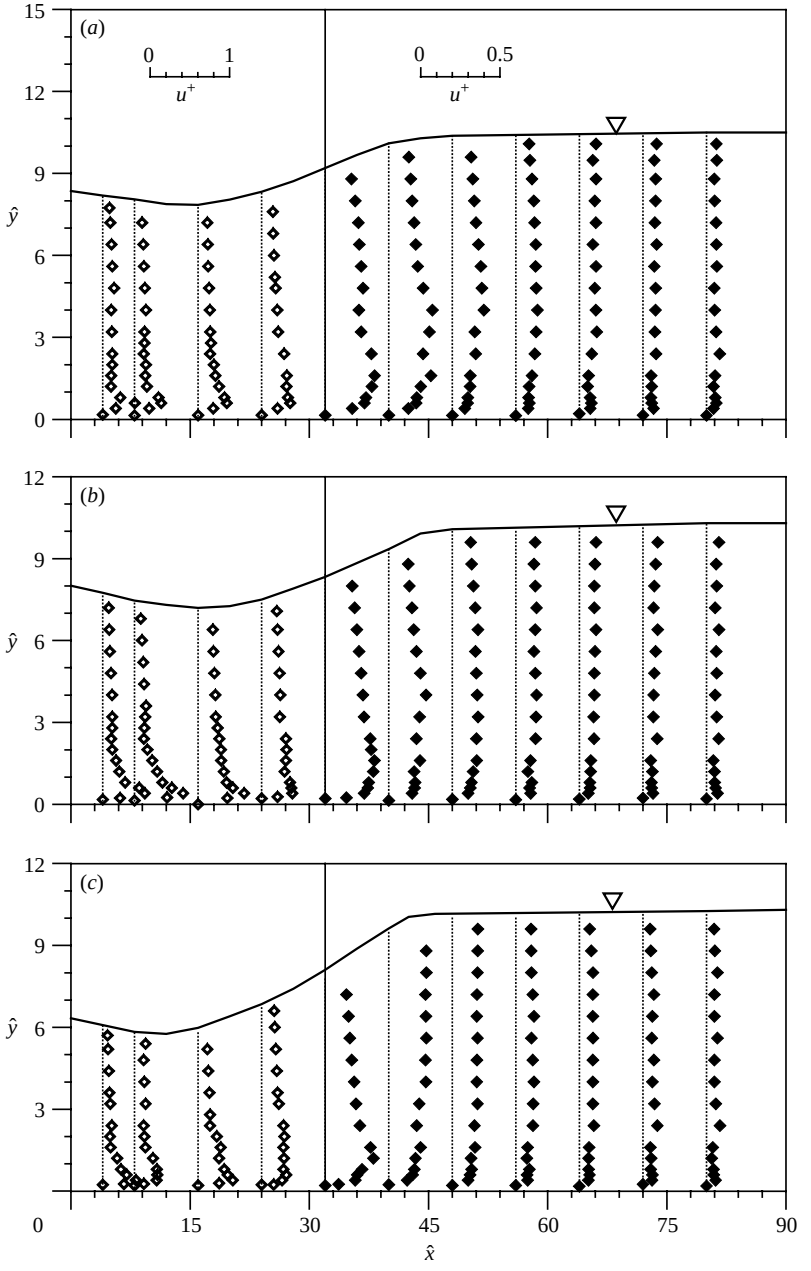

FIGURE 5. Vertical profiles of u^+ for $U = 1.435\,\mathrm{m\,s^{-1}}$, $L = 0.4\,\mathrm{m}$ and $b = 12.5\,\mathrm{mm}$: (*a*) $\varepsilon = 0.8\,\mathrm{mm}$, (*b*) $\varepsilon = 1.86\,\mathrm{mm}$ and (*c*) $\varepsilon = 3\,\mathrm{mm}$.

streamwise distance $\hat{x}$ up to an overall maximum at the middle of the smooth bed and then decreases gradually towards the recovering zone on the rough beds.

Figure 6 shows the vertical profiles of non-dimensional vertical turbulence intensity component $v^+ (= (\overline{v'v'})^{0.5}/U$, where v' is the fluctuation of v) at different $\hat{x}$ in submerged wall jets on a rigid bed with abrupt changes from smooth to rough beds. In the profiles of v^+, bulges are evident at the mid flow depth except near the

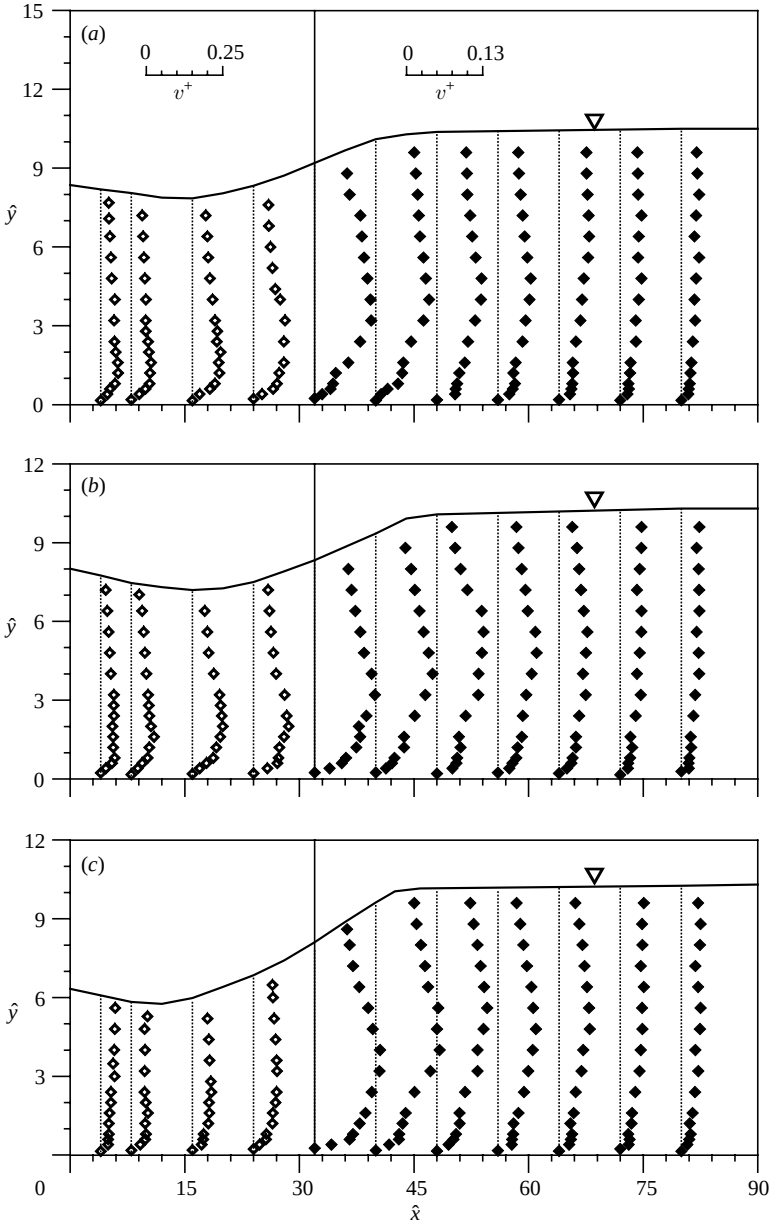

FIGURE 6. Vertical profiles of v^+ for $U = 1.435\,\mathrm{m\,s^{-1}}$, $L = 0.4\,\mathrm{m}$ and $b = 12.5\,\mathrm{mm}$: (*a*) $\varepsilon = 0.8\,\mathrm{mm}$, (*b*) $\varepsilon = 1.86\,\mathrm{mm}$ and (*c*) $\varepsilon = 3\,\mathrm{mm}$.

sluice opening. The influence of roughness is prominent as, in the fully developed and recovering zones, the magnitude of v^+ of a particular profile increases with increase in roughness ε. However, v^+ increases with increase in $\hat{x}$ up to the junction of the smooth and rough beds and then decreases to attain a constant profile in the recovering zone.

3.3. *Decay of submerged wall jet*

Figure 1(*c*) shows schematic profiles of the horizontal velocity component in a submerged wall jet. The local maximum jet velocity u_0, which is the maximum velocity

of an individual vertical profile of u at any distance x, decreases with increase in streamwise distance x due to an increase in boundary layer thickness δ. In order to represent the decay of a submerged wall jet in the streamwise direction due to abrupt changes from smooth to rough beds, the functional representations of the variations of local maximum velocity u_0 and boundary layer thickness δ along streamwise distance x are given by

$$u_0(x \leqslant L) = u_0(U, b, x, \nu), \quad u_0(x > L) = u_0(U, b, x - L, \varepsilon), \tag{3.1a}$$

$$\delta(x \leqslant L) = \delta(U, b, x, \nu), \quad \delta(x > L) = \delta(U, b, x - L, \varepsilon), \tag{3.1b}$$

where ν is the kinematic viscosity of the fluid. Applying dimensional analysis, the non-dimensional equations for u_0 and δ, whose coefficients and exponents were derived by multiple linear regression analysis using all the experimental data collected by the ADV, are.

$$\hat{u}_0(\hat{x} \leqslant \hat{L}) = 1 - 0.235\hat{x}^{0.4}R^{-0.05}, \quad \hat{u}_0(\hat{x} > \hat{L}) = 1 - 0.1(\hat{x} - \hat{L})^{0.55}\hat{\varepsilon}^{0.05}, \tag{3.2a}$$

$$\hat{\delta}(\hat{x} \leqslant \hat{L}) = 0.27(\hat{x} + 11.2)^{0.72}R^{-0.2}, \quad \hat{\delta}(\hat{x} > \hat{L}) = 0.21(\hat{x} - \hat{L})^{0.75}\hat{\varepsilon}^{0.25}, \tag{3.2b}$$

where $\hat{u}_0 = u_0/U$, $\hat{L} = L/b$, R is the Reynolds number of the issuing jet ($= Ub/\nu$), $\hat{\varepsilon} = \varepsilon/b$ and $\hat{\delta} = \delta/b$. Note that the term $(\hat{x} + 11.2)$, in (3.2*b*), is important in computation of the boundary layer thickness, because the virtual origin of the boundary layer of a jet is at $x = -11.2\,b$ where $\delta = 0$ (Schwarz & Cosart 1961). Equations (3.2*a*) and (3.2*b*) indicate that the maximum jet velocity u_0 diminishes and the boundary layer thickness δ increases with increase in streamwise distance x.

4. Reynolds stress profiles

4.1. *Theoretical Reynolds stress*

The two-dimensional Navier–Stokes equations of a steady turbulent flow are given in non-dimensional form (Rajaratnam 1976) as

$$\hat{u}\frac{\partial \hat{u}}{\partial \hat{x}} + \hat{v}\frac{\partial \hat{u}}{\partial \hat{y}} = -\frac{\partial \hat{p}}{\partial \hat{x}} + \frac{1}{R}\left(\frac{\partial^2 \hat{u}}{\partial \hat{x}^2} + \frac{\partial^2 \hat{u}}{\partial \hat{y}^2}\right) - \frac{\partial u^{+2}}{\partial \hat{x}} - \frac{\partial uv^{+}}{\partial \hat{y}}, \tag{4.1}$$

$$\hat{u}\frac{\partial \hat{v}}{\partial \hat{x}} + \hat{v}\frac{\partial \hat{v}}{\partial \hat{y}} = -\frac{\partial \hat{p}}{\partial \hat{y}} + \frac{1}{R}\left(\frac{\partial^2 \hat{v}}{\partial \hat{x}^2} + \frac{\partial^2 \hat{v}}{\partial \hat{y}^2}\right) - \frac{\partial v^{+2}}{\partial \hat{y}} - \frac{\partial uv^{+}}{\partial \hat{x}}, \tag{4.2}$$

where $\hat{p} = p/(\rho U^2)$, p is the piezometric pressure, ρ is the mass density of fluid and uv^{+} is the non-dimensional Reynolds stress, that is $-\overline{u'v'}/U^2$. The continuity equation is

$$\frac{\partial \hat{u}}{\partial \hat{x}} + \frac{\partial \hat{v}}{\partial \hat{y}} = 0. \tag{4.3}$$

Since $\hat{u} \gg \hat{v}$, velocity and stress gradients in the y-direction are much greater than those in the x-direction. Thus, (4.2) becomes $\partial p/\partial y = -\partial v^{+2}/\partial \hat{y}$ (Townsend 1956; Rajaratnam 1976). Therefore, from (4.1) one can write

$$\hat{u}\frac{\partial \hat{u}}{\partial \hat{x}} + \hat{v}\frac{\partial \hat{u}}{\partial \hat{y}} + \frac{\partial}{\partial \hat{x}}(u^{+2} - v^{+2}) + \frac{\partial uv^{+}}{\partial \hat{y}} = \frac{1}{R}\frac{\partial^2 \hat{u}}{\partial \hat{y}^2}. \tag{4.4}$$

The general characteristic feature of the flow in submerged wall jets is self-preserving (see § 6). Therefore, the following functional relationships can be considered for the solution of (4.4):

$$\hat{u} = \hat{u}_0\,\psi(\eta), \quad u^{+2} = \hat{u}_0^2\,\phi_1(\eta), \quad v^{+2} = \hat{u}_0^2\,\phi_2(\eta), \quad uv^{+} = -\hat{u}_0^2\,\xi(\eta), \tag{4.5}$$

ε (mm)	c	α	β	σ
Smooth bed	−1.41	7.81	1.308	0.641
0.8	−1.12	5.42	1.048	0.426
1.86	−0.93	5.05	0.862	0.412
3	−0.9	4.95	0.642	0.397

TABLE 2. Values of coefficient and exponents in equations (4.8), (4.9) and (5.1).

where $\eta = y/\delta$. Substituting (4.5) into (4.4), one obtains

$$\frac{\hat{\delta}}{\hat{u}_0}\frac{\partial \hat{u}_0}{\partial \hat{x}}\psi^2 - \frac{1}{\hat{u}_0}\frac{\mathrm{d}(\hat{u}_0\hat{\delta})}{\mathrm{d}\hat{x}}\frac{\mathrm{d}\psi}{\mathrm{d}\eta}\int_0^\eta \psi\,\mathrm{d}\eta + 2\frac{\hat{\delta}}{\hat{u}_0}\frac{\mathrm{d}\hat{u}_0}{\mathrm{d}\hat{x}}\phi_1 - \frac{\mathrm{d}\hat{\delta}}{\mathrm{d}\hat{x}}\eta\frac{\mathrm{d}\phi_1}{\mathrm{d}\eta} + \frac{\mathrm{d}\hat{\delta}}{\mathrm{d}\hat{x}}\eta\frac{\mathrm{d}\phi_2}{\mathrm{d}\eta} - 2\phi_2\frac{\hat{\delta}}{\hat{u}_0}\frac{\mathrm{d}\hat{u}_0}{\mathrm{d}\hat{x}} - \frac{\mathrm{d}\xi}{\mathrm{d}\eta} = \frac{1}{R}\frac{\mathrm{d}^2\psi}{\mathrm{d}\eta^2}. \quad (4.6)$$

Inserting the functional relationships for ψ, ϕ_1, ϕ_2 and ξ given in (4.5) into (4.6) and then integrating (neglecting the viscous term), the expression for the non-dimensional Reynolds stress uv^+ is obtained as

$$uv^+ = -\hat{u}_0\hat{\delta}\frac{\mathrm{d}\hat{u}_0}{\mathrm{d}\hat{x}}\int_\eta^{\hat{h}}\psi^2\mathrm{d}\eta - \hat{u}_0\left(\hat{\delta}\frac{\mathrm{d}\hat{u}_0}{\mathrm{d}\hat{x}} + \hat{u}_0\frac{\mathrm{d}\hat{\delta}}{\mathrm{d}\hat{x}}\right)\left(\int_\eta^{\hat{h}}\psi^2\mathrm{d}\eta + \psi\int_0^\eta \psi\,\mathrm{d}\eta\right) \quad (4.7)$$

where $\hat{h} = h/b$ and h is the flow depth at any x. From the similarity of the profiles of u at different streamwise distances x, one can determine $\psi = \psi(\eta)$. Equations for ψ are obtained from the least square fitting of all the experimental data in the fully developed zone as

$$\psi(\eta \leqslant 1) = \eta^{1/\alpha}, \quad (4.8)$$

$$\psi(\eta > 1) = \exp[c(\eta - 1)^{0.95}], \quad (4.9)$$

where α and c are the exponent and coefficient, respectively, being dependent on the roughness ε of the beds. Table 2 furnishes the values of the exponent α and the coefficient c for different ε. For flow on a smooth bed, the value of α is close to that in a turbulent boundary layer, where it lies between 7 and 10 (Dey 2002). Using the expressions for $\hat{u}_0$, $\hat{\delta}$ and ψ in (4.7), profiles of uv^+ are computed. Figure 7 shows the vertical profiles of computed uv^+.

4.2. *Experimental Reynolds stress*

Figure 7 displays the vertical profiles of non-dimensional Reynolds stress uv^+ at different $\hat{x}$ in submerged wall jets on a rigid bed with abrupt changes from smooth to rough beds. The Reynolds stress uv^+ near the bed is positive and reduces sharply, changing its sign to negative and forming weak bulges (maximum negative value of uv^+ in a vertical profile) with increase in vertical distance $\hat{y}$ due to the surface roller on the smooth bed. The bulges in the profiles of uv^+ gradually disappear with increase in $\hat{x}$, especially on the rough beds. However, in the recovering zone, as uv^+ is weak (in comparison with uv^+ in the fully developed zone) it is almost constant along the vertical. It is apparent from the comparison between the experimental data and computed profiles of uv^+, in figure 7, that there is a difference in the data in some profiles in the recovering zone. This is attributed to uv^+ being computed from

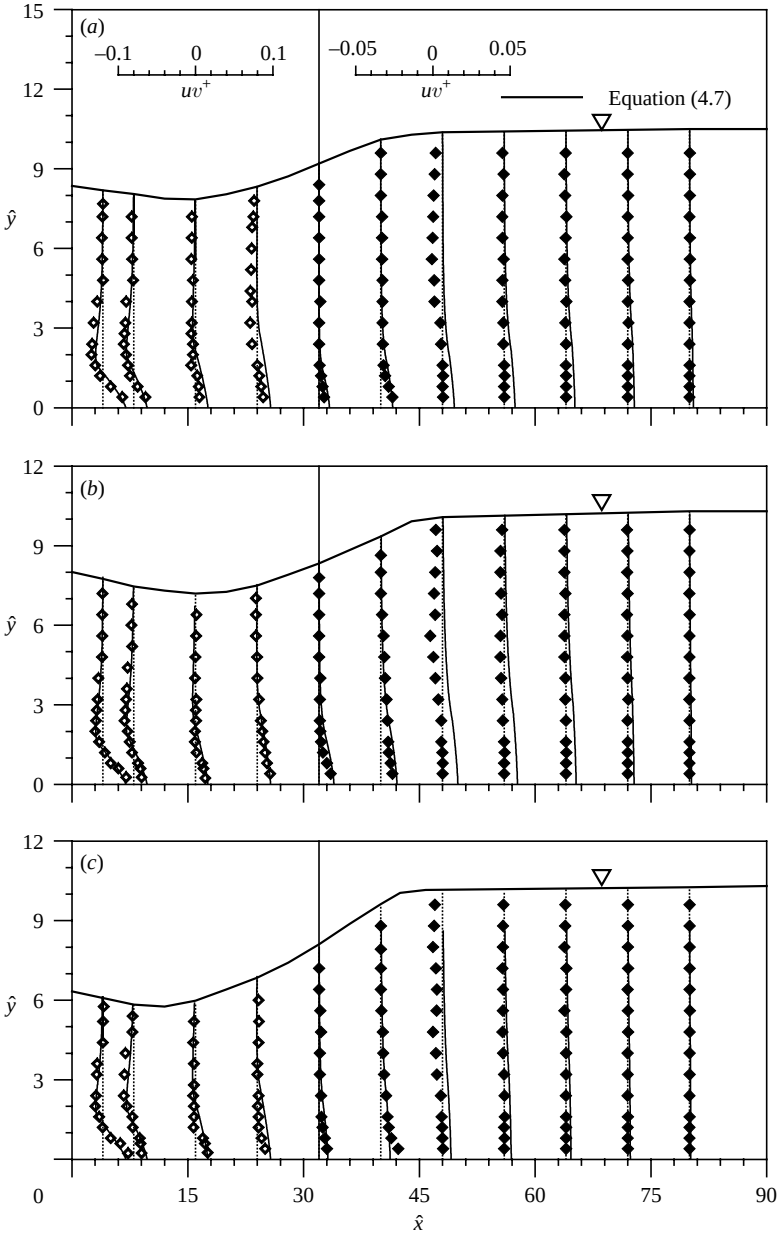

FIGURE 7. Vertical profiles of Reynolds stress uv^+ for $U = 1.435\,\mathrm{m\,s^{-1}}$, $L = 0.4\,\mathrm{m}$ and $b = 12.5\,\mathrm{mm}$: (*a*) $\varepsilon = 0.8\,\mathrm{mm}$, (*b*) $\varepsilon = 1.86\,\mathrm{mm}$ and (*c*) $\varepsilon = 3\,\mathrm{mm}$.

(4.7), which is dependent on $\hat{u}_0$, $\hat{\delta}$ and ψ determined empirically (see 3.2(*a*), 3.2(*b*), (4.8) and (4.9)) from experimental data that are independent of the experimental data for uv^+. In addition, having used a number of empirically determined parameters, a perfect matching between the experimental data and the computed results is difficult. However, the computed profiles of uv^+ agree reasonably with the experimental data.

5. Bed shear stress

5.1. *Theoretical bed shear stress*

Inserting (4.3) and (4.5) into (4.4) and integrating the resulting equation, the following expression for the non-dimensional bed shear stress is obtained:

$$\hat{\tau} = -\left(2\hat{\delta}\hat{u}_0\frac{\mathrm{d}\hat{u}_0}{\mathrm{d}\hat{x}} + \hat{u}_0^2\frac{\mathrm{d}\hat{\delta}}{\mathrm{d}\hat{x}}\right)\int_0^{\eta}(\psi^2 + \phi_1 - \phi_2)\,\mathrm{d}\eta \tag{5.1}$$

where $\hat{\tau} = \tau/(\rho U^2)$. To solve (5.1), one requires information on $\phi_1(\eta)$ and $\phi_2(\eta)$. Therefore, the expressions for $\phi_1 = \eta^{1/\beta}$ and $\phi_2 = \eta^{1/\sigma}$ are obtained from least-square fitting of the present experimental data. The exponents β and σ are functions of bed roughness ε. Table 2 furnishes the values of exponents β and σ for different ε determined from the least-square fitting of all the experimental data in the fully developed zone. The bed shear stress $\hat{\tau}$ is computed from (5.1), using the expressions for $\hat{u}_0$, $\hat{\delta}$, ψ, ϕ_1 and ϕ_2. The computed horizontal distributions of $\hat{\tau}$ are shown in figure 8.

5.2. *Experimental bed shear stress*

Experimental values of the bed shear stress τ are estimated from the Reynolds stress profiles extending on to the bed level, as was done by Dey & Lambert (2005). The non-dimensional bed shear stress is, therefore, given by

$$\hat{\tau} = uv^+|_{\eta=0}. \tag{5.2}$$

Figure 8 shows the distributions of non-dimensional bed shear stress $\hat{\tau}$ along streamwise direction $\hat{x}$. Bed shear stress $\hat{\tau}$ decreases with increase in streamwise distance $\hat{x}$; and the change in $\hat{\tau}$ at the junction of smooth and rough beds is basically gradual, though a slight discontinuity is observed in the computed curves. It is evident from the comparison of the experimental data and computed curves that there is a tendency to overestimate the bed shear stress. The discrepancy between the experimental and the computed values of $\hat{\tau}$ results from the experimental scatter. It may be noted that $\hat{\tau}$ is determined from the Reynolds stress profiles, which are sensitive to the turbulent fluctuations and hence subject to uncertain attenuation and error, especially near the bed. Nevertheless, in general, collapse of the experimental data and the computed curves is reasonable on rough beds.

6. Flow characteristics of submerged wall jets over abrupt changes from smooth to rough beds

6.1. *Determination of length scale*

For the local maximum jet velocity u_0, the length scale λ, which groups the data of all major flow characteristics, is the distance from the sluice opening at which $u_0 = U/2$. Long *et al.* (1990) used the following relationship for λ for smooth bed:

$$\frac{\lambda}{b} = \frac{49}{1 + C_1(\mathrm{d}h/\mathrm{d}x)_\lambda F^{-2}} \tag{6.1}$$

where C_1 is a coefficient. For the combination of smooth and rough beds, the free-surface slope, that is $(\mathrm{d}h/\mathrm{d}x)_\lambda$, at $x = \lambda$ is a function of S, L and ε, as shown in figures 9(*a*) and 9(*b*). Using the least-square curve fitting, the following relationship for different L and ε is obtained:

$$\left(\frac{\mathrm{d}h}{\mathrm{d}x}\right)_\lambda = C_2 \times 10^{-KS} \tag{6.2}$$

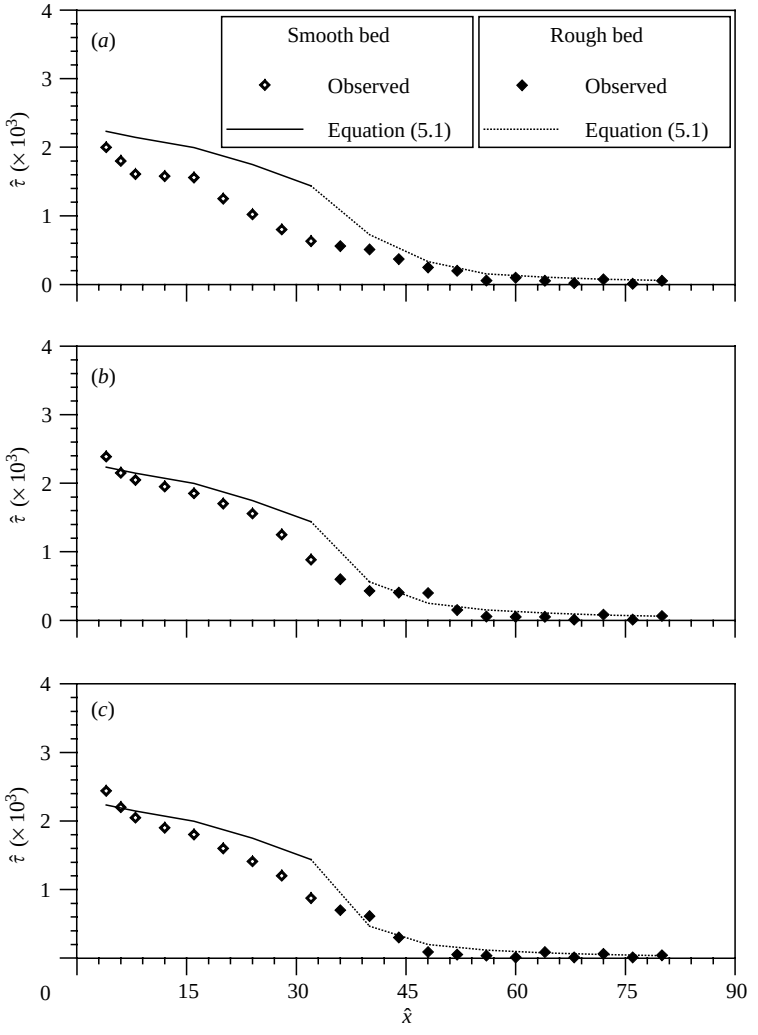

FIGURE 8. Horizontal distributions of bed shear stress $\hat{\tau}$ for $U = 1.435\,\mathrm{m\,s^{-1}}$, $L = 0.4\,\mathrm{m}$ and $b = 12.5\,\mathrm{mm}$: (*a*) $\varepsilon = 0.8\,\mathrm{mm}$, (*b*) $\varepsilon = 1.86\,\mathrm{mm}$ and (*c*) $\varepsilon = 3\,\mathrm{mm}$.

where C_2 and K are the coefficients and exponents, respectively, being dependent on L and ε. Substituting (6.2) in (6.1), one can write

$$\frac{\lambda}{b} = \frac{49}{1 + C \times 10^{-KS} F^{-2}} \tag{6.3}$$

where coefficient C is the product of C_1 and C_2. The values of C for different L and ε are determined from the least-square curve fitting of the plots of λ/b versus $10^{-KS}F^{-2}$ as shown in figures 9(*c*) and 9(*d*). The dependence of C and K on relative roughness $\hat{\varepsilon}$ for different L is given in figures 9(*e*) and 9(*f*), respectively.

Barring the horizontal length scale λ, the vertical length scale y_1 for velocity u, shown in figure 10(*a*), is used to collapse the vertical distributions of $\hat{u}$ onto a single band. It is the vertical distance y where $u = u_0/2$ and $\partial u/\partial y < 0$. Moreover, the vertical length scale y_2 for the Reynolds stress $-\overline{u'v'}$, shown in figure 10(*b*), being the vertical

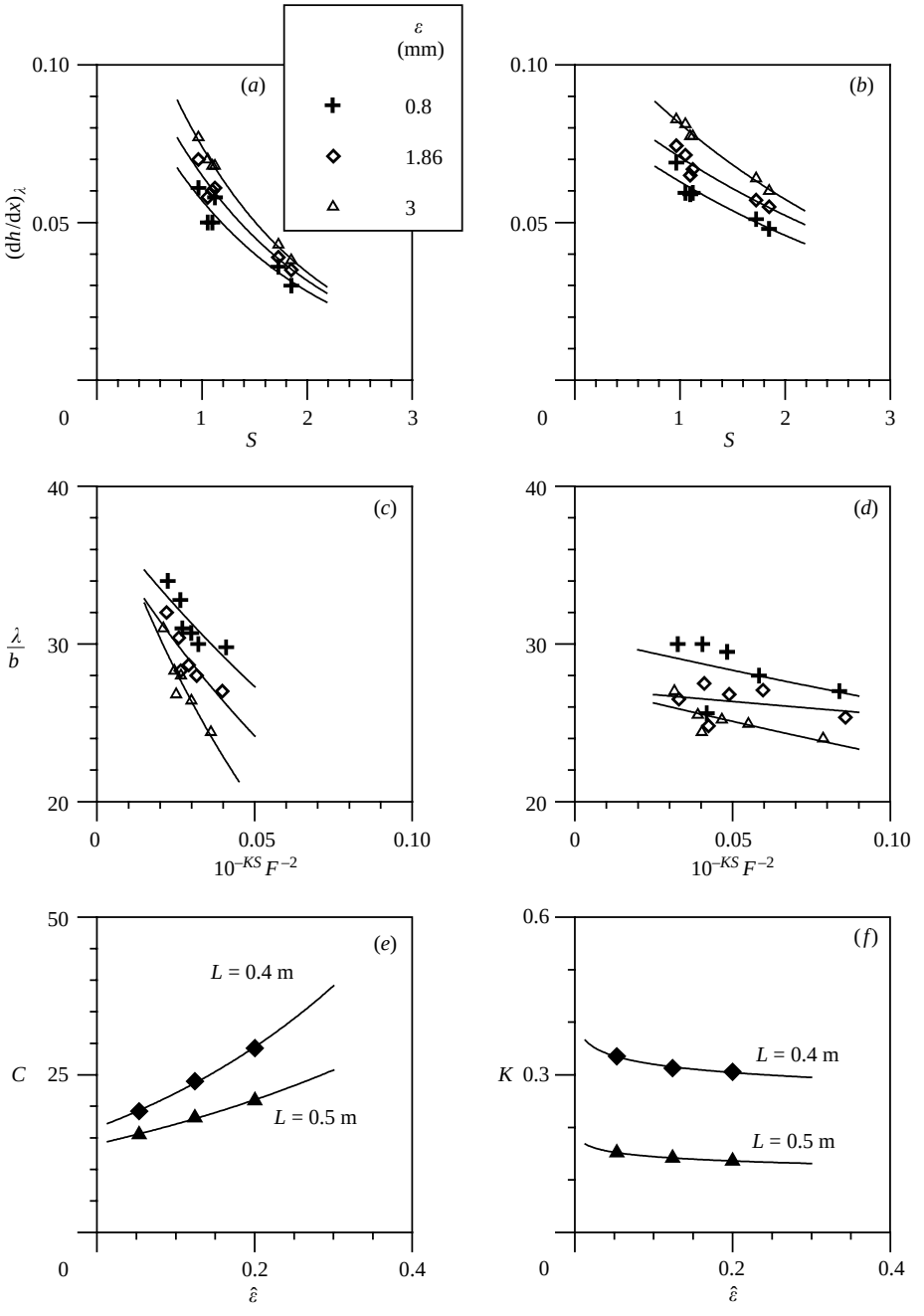

FIGURE 9. (*a*) $(dh/dx)_\lambda$ as a function of S for $L = 0.4$ m, (*b*) $(dh/dx)_\lambda$ as a function of S for $L = 0.5$ m, (*c*) λ/b as a function of $10^{-KS}F^{-2}$ for $L = 0.4$ m, (*d*) λ/b as a function of $10^{-KS}F^{-2}$ for $L = 0.5$ m, (*e*) variation of C with $\hat{\varepsilon}$ and (*f*) variation of K with $\hat{\varepsilon}$.

distance y where $\overline{u'v'} = (\overline{u'v'})_0/2$ and $\partial(\overline{u'v'})/\partial y < 0$, is considered to group the vertical distributions of uv^+ together. Subscript 0 refers to a local maximum value in a vertical profile. Furthermore, for the null-point of the Reynolds stress profiles, $y = \delta_1$ where $\overline{u'v'} = 0$ and $\partial(\overline{u'v'})/\partial y > 0$.

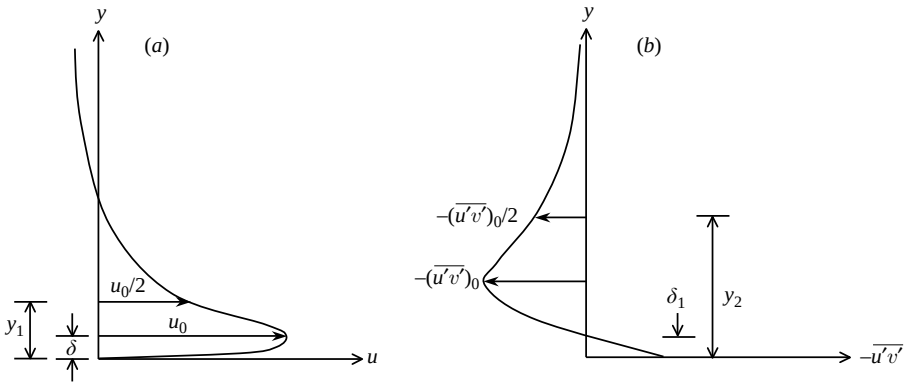

FIGURE 10. (*a*) Schematic velocity profile and (*b*) schematic Reynolds stress profile.

6.2. *Flow characteristics*

The decay of non-dimensional maximum velocity u_0/U, in the fully developed zone, over non-dimensional streamwise distance $\tilde{x}(=x/\lambda)$ in a submerged wall jets over an abrupt change from smooth to rough beds having different roughness ε, is represented in figure 11(*a*) for the smooth bed length $L = 0.5$ m. Different symbols are used to represent the data for smooth and rough beds. The use of a common length scale λ for the flow over smooth and rough beds, makes it possible for all the data to collapse reasonably on a single band (which means that the data have a definite mean trend), though in the vicinity of the junction of the smooth and rough beds ($\tilde{x} \geqslant 1$) a little data scatter exists due to the abrupt changes of bed roughness. To be more explicit, the abrupt change of bed roughness reduces the magnitude of maximum velocity u_0 drastically due to the additional resistance resulting in a locally dispersed trend. However, the effect of the bed roughness is also noticeable from the free-surface profiles (see figure 4), as there is a considerable depression of the free-surface elevation over the smooth bed with increasing bed roughness. A comparative study of the present data trend with the curves of a wall jet (Rajaratnam 1976), free jump (Rajaratnam 1965) and submerged jet on a smooth bed (Long *et al.* 1990) reveals that the mean trend of u_0/U versus $\tilde{x}$ data for submerged wall jets on a smooth bed coincides with the curves of a free jump and a submerged jet on a smooth bed. However, upstream of the junction of smooth and rough beds, the data trend differ. All the data of a rough bed lie well below the curves of a free jump and submerged jet on smooth bed. Hence, one can conclude that the decay rate of local maximum velocity u_0, being significantly influenced by the bed roughness ε, increases on rough beds; and the flow is self-preserving on smooth and rough beds. It is revealed from data not shown (to restrict the number of figures) for $L = 0.4$ mm that a decrease of the length L of the smooth bed expedites the decay rate for obvious reasons. Importantly, the use of the same length scale λ also makes it possible to collapse the data of $(uv^+)_0/(uv^+)_m$, $(u^+)_0/(u^+)_m$ and $(v^+)_0/(v^+)_m$ approximately onto a single band, as shown in figures 11(*b*), 12(*a*) and 12(*b*), respectively, though as usual there is a little data scatter in the vicinity of the junction of smooth and rough beds. Here, subscript m refers to a maximum for an experimental condition. The comparisons show that the present data trends have good agreement with the curve of a submerged jet on a smooth bed in the smooth bed region, but they lie below the curve of a submerged jet on smooth bed in the rough bed region due to the roughness effect. Therefore,

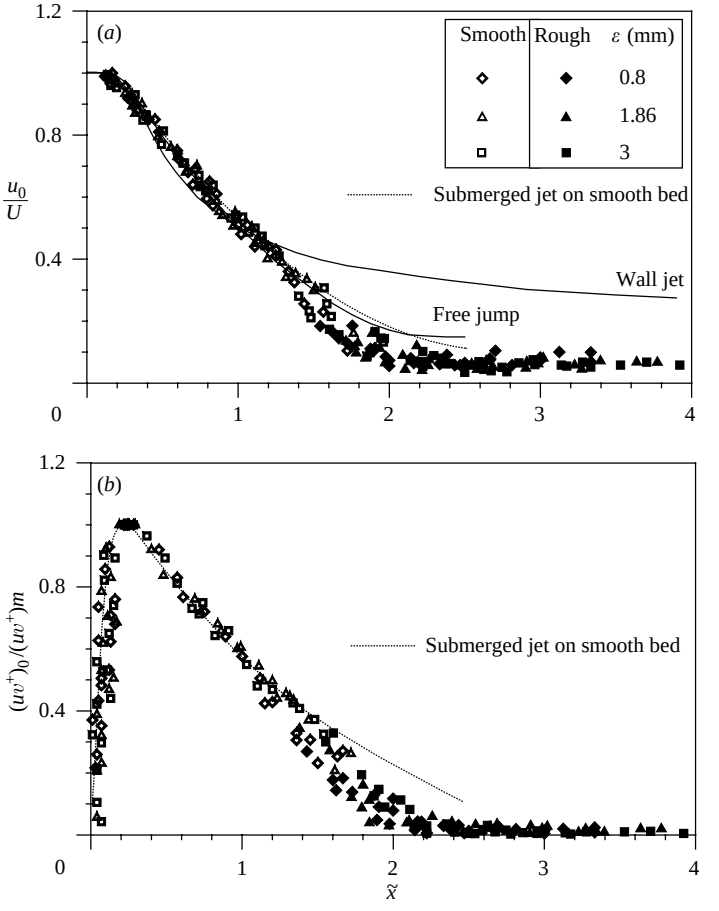

FIGURE 11. (*a*) u_0/U as a function of $\tilde{x}$ and (*b*) dependence of $(uv^+)_0/(uv^+)_m$ on $\tilde{x}$, for different ε and $L = 0.5$ m.

the rates of decay of $(uv^+)_0$, $(u^+)_0$ and $(v^+)_0$ on rough beds are faster than those on smooth beds, as a result of mixing of fluid caused by the roughness.

To assess the degree of similarity in the individual profiles of u in the fully developed zone, using u_0 and y_1 as the scales, the profiles of non-dimensional horizontal velocity u/u_0 are plotted against non-dimensional vertical distance $\tilde{y}$ $(= y/y_1)$ in figures 13(*a*) and 13(*b*) for smooth and rough bed regions, respectively. In figure 13(*a*), the collapse of the velocity data and the curves for the wall jet and submerged jet on smooth bed is good up to $\tilde{y} = 1.5$ for different downstream roughness ε. The velocity data depart from the wall jet curve in the outer layer for $\tilde{y} > 1.5$. The negative magnitude of u/u_0 in the outer-layer profiles indicates the region of reversed flow. In the upper portion of the outer layer, the mean data trend lies between the curves of the wall jet and submerged jet on smooth bed. For the flow on a rough bed, the profiles of u/u_0, in the inner layer, are influenced by the bed roughness (see figure 13*b*). In reality, the bed roughness increases the inner-layer thickness of individual velocity profiles. Hence, the rough bed data near the bed are less 'full' compared to the curves of the wall jet and submerged jet on the smooth bed. The data of $uv^+/(uv^+)_0$ versus ζ $(= (y - \delta_1)/(y_2 - \delta_1))$, $u^+/(u^+)_0$ versus $z(= y/y_2)$ and $v^+/(u^+)_0$ versus z are plotted in figures 14–16 illustrating the degrees of similarity that exist in the individual profiles

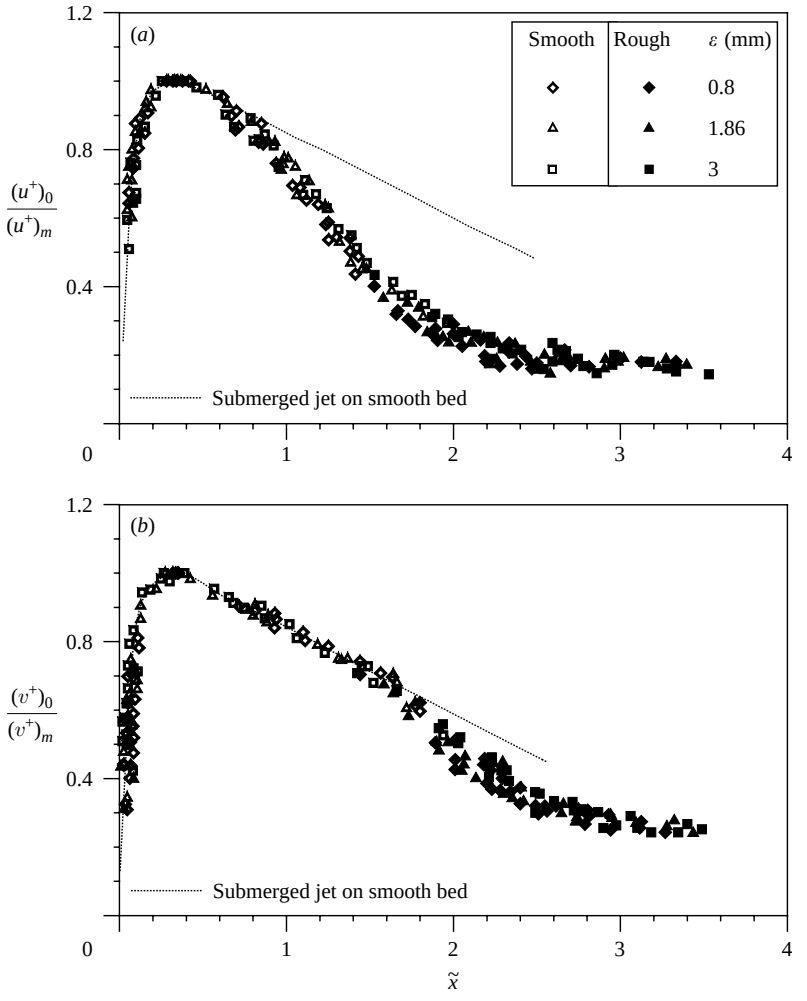

FIGURE 12. (*a*) Dependence of $(u^+)_0/(u^+)_\mathrm{m}$ and (*b*) dependence of $(v^+)_0/(v^+)_\mathrm{m}$ on $\tilde{x}$ for different ε and $L = 0.5$ m.

of uv^+, u^+ and v^+ in the fully developed zone on smooth and rough beds. The data of smooth bed regions and the curves of the submerged jet on a smooth bed collapse in the inner layer (figures 14*a*, 15*a* and 16*a*). On the other hand, as a result of increasing turbulence intensity on account of the roughness, the data of $(u^+)_0$ and $(v^+)_0$ of rough bed regions lie in between the curves of wall jet and submerged jet on a smooth bed in the inner layer (figures 14*b* and 15*b*); whereas the data of $(uv^+)_0$ of rough bed regions (figure 16*b*), being sagging in nature, intercept wall jet curve at $\zeta = 0.05$. However, in the outer layer, the data of smooth and rough bed regions are closer to the curves of the wall jet. To be more explicit, the roughness ε augments the inner-layer thickness of the u^+ and v^+ profiles.

The streamwise variations of non-dimensional vertical length scale y_1/b for horizontal velocity component u are shown in figure 17(*a*) for $L = 0.5$ m. It shows that the jet half-widths on smooth and rough beds decay slower and faster than that in a classical wall jet, respectively. Therefore, the jet half-width is influenced significantly by an abrupt change of bed roughness. However, the data lie well below the curves of

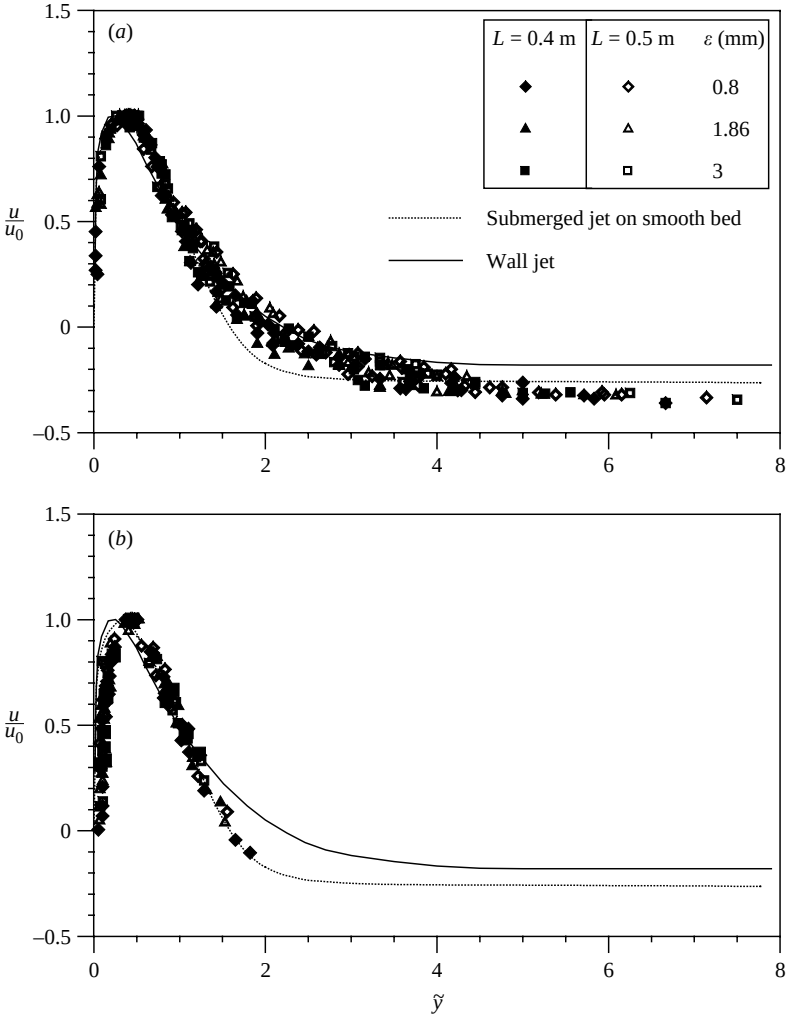

FIGURE 13. (*a*) u/u_0 as a function of $\tilde{y}$ in fully developed zone of smooth beds for different downstream ε and L ($L = 0.4$ m (data range: $3.3 \leqslant \hat{x} \leqslant 20$) and 0.5 m (data range: $3.3 \leqslant \hat{x} \leqslant 26.7$)) and (*b*) u/u_0 as a function of $\tilde{y}$ in fully developed zone of rough beds for different ε and upstream L ($L = 0.4$ m (data range: $26.7 \leqslant \hat{x} \leqslant 40$) and 0.5 m (data range: $33.3 \leqslant \hat{x} \leqslant 40$)).

a free jump and submerged jet on a smooth bed. Figure 17(*b*) presents the change of y_2/b with $\hat{x}$, which is the decay of half-widths of the Reynolds stress in the streamwise direction. The half-widths of the Reynolds stress on smooth and rough beds decays slower than those in the wall jet and submerged jet on smooth bed. It is seen from the plot of δ_1/b versus $\hat{x}$, in figure 17(*b*), that the null-points of the Reynolds stress profiles in smooth and rough beds remain similar to those in a submerged jet on a smooth bed.

7. Modelling of scour downstream of an apron

7.1. *Experimental observation on the scour process*

The scouring process downstream of an apron due to submerged jets issuing from a sluice opening is a multifaceted phenomenon owing to the abrupt change of

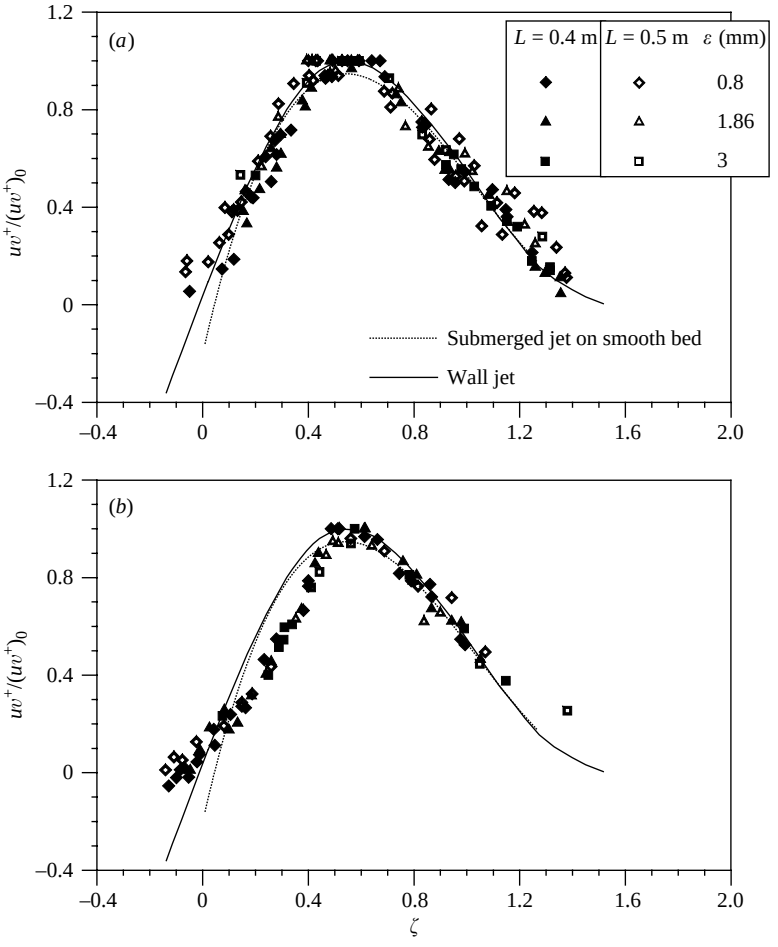

FIGURE 14. (*a*) Similarity of distributions of uv^+ in fully developed zone of smooth beds for different downstream ε and L ($L = 0.4$ m (data range: $3.3 \leqslant \hat{x} \leqslant 20$) and 0.5 m (data range: $3.3 \leqslant \hat{x} \leqslant 26.7$)) and (*b*) similarity of distributions of uv^+ in fully developed zone of rough beds for different ε and L ($L = 0.4$ m (data range: $26.7 \leqslant \hat{x} \leqslant 40$) and 0.5 m (data range: $33.3 \leqslant \hat{x} \leqslant 40$)).

the flow characteristics (including free-surface profile) on the sediment bed with time (figure 18*a*). The sediment bed following a smooth rigid apron of length L was initially planar and the submerged jet flowed in a direction parallel to the bed surface. It is important to mention that the increased depression of the free surface in the presence of the sediment bed (that is the rough bed) downstream of an apron, apparent in figure 4, enhanced the erosive power of the submerged jet. Scour starts at the downstream edge of the apron when the bed shear stress induced by the submerged wall jet exceeds the threshold bed shear stress for sediment movement. The evolution of the vertical dimension of the scour hole was faster than the longitudinal one. In the initial stage, the suspension of sediment, in addition to the bed-load, was the main means of sediment transport. But with the increase of the vertical dimension of the scour hole, the mode of sediment transport changed to bed-load only. The down-slope sliding and rolling movement of sediment took place when the bed shear stress induced by the submerged wall jet was reduced considerably with the development of the scour hole.

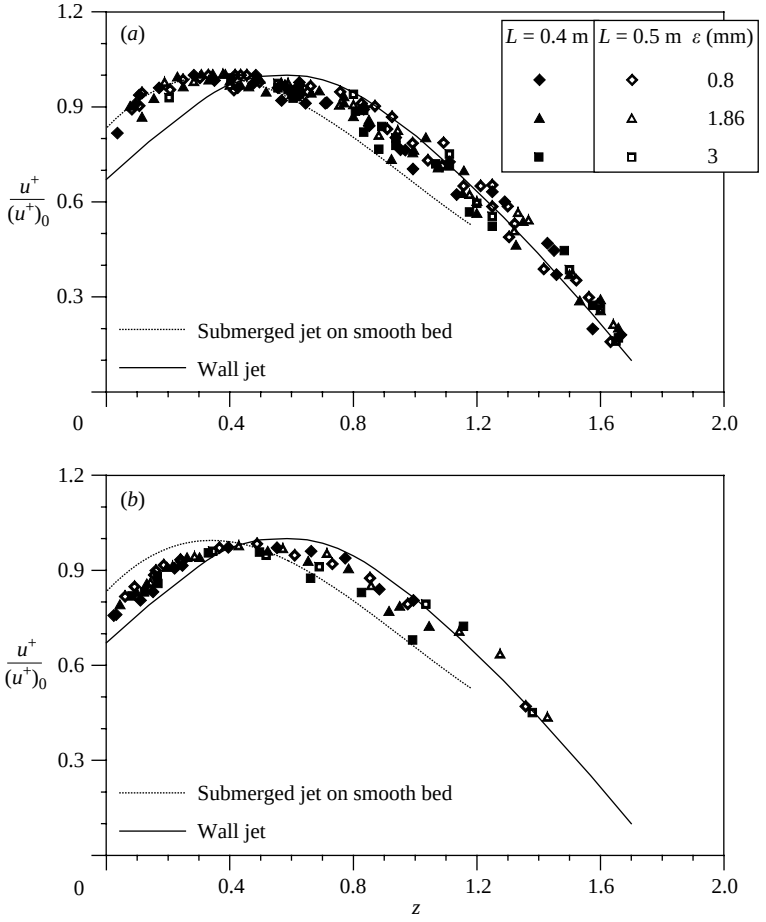

FIGURE 15. (*a*) Similarity of distributions of u^+ in fully developed zone of smooth beds for different downstream ε and L ($L = 0.4$ m (data range: $3.3 \leqslant \hat{x} \leqslant 20$) and 0.5 m (data range: $3.3 \leqslant \hat{x} \leqslant 26.7$)) and (*b*) similarity of distributions of u^+ in fully developed zone of rough beds for different ε and L ($L = 0.4$ m (data range: $26.7 \leqslant \hat{x} \leqslant 40$) and 0.5 m (data range: $33.3 \leqslant \hat{x} \leqslant 40$)).

The upstream side of the scour hole achieved a steeper slope than the downstream side. However, after a considerable period of time, equilibrium was reached, when the sediment particles at the surface of the scour hole remained at the threshold condition.

7.2. *Equilibrium of sediment particles*

The forces acting on a sediment particle lying on the equilibrium scoured bed, shown in figure 18(*a*), are the drag force F_D, lift force F_L, and submerged weight of a sediment particle F_G. Based on these forces, the threshold condition of a sediment particle resting on a bed slope θ (streamwise) can be defined by the following equation:

$$\tilde{\tau}_c = \cos\theta \left(1 + \frac{\tan\theta}{\mu}\right) \tag{7.1}$$

where $\tilde{\tau}_c = [\tau_c]_{\theta=\theta}/[\tau_c]_{\theta=0}$, $\theta = \arctan(\mathrm{d}y/\mathrm{d}x)$, μ is the Coulomb frictional coefficient of sediment, equalling $\tan\phi$, and ϕ is the angle of repose of sediment. Subscript 'c'

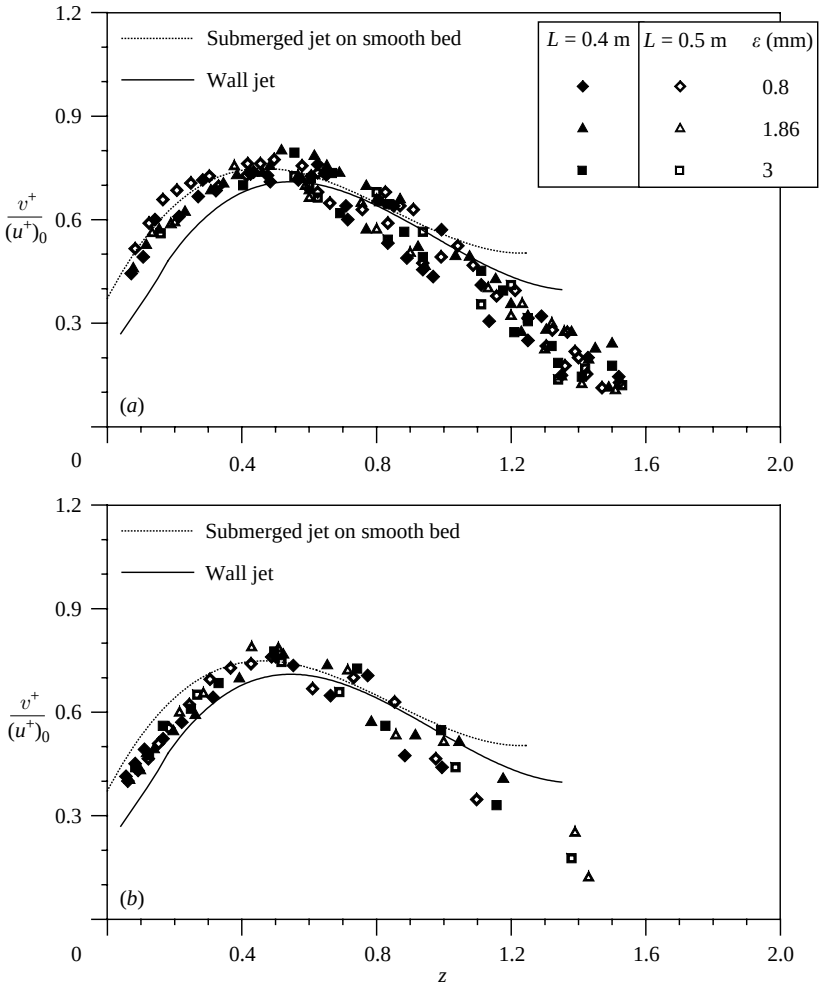

FIGURE 16. (*a*) Similarity of distributions of v^+ in fully developed zone of smooth beds for different downstream ε and L ($L = 0.4$ m (data range: $3.3 \leqslant \hat{x} \leqslant 20$) and 0.5 m (data range: $3.3 \leqslant \hat{x} \leqslant 26.7$)) and (*b*) similarity of distributions of v^+ in fully developed zone of rough beds for different ε and L ($L = 0.4$ m (data range: $26.7 \leqslant \hat{x} \leqslant 40$) and 0.5 m (data range: $33.3 \leqslant \hat{x} \leqslant 40$)).

refers to the threshold or critical condition. The threshold bed shear stress $[\tau_c]_{\theta=0}$ for uniform sediment on a horizontal bed ($\theta = 0$) can be obtained mathematically from the model given by Dey (1999). The most accurate curve for the determination of threshold bed shear stress was given by Yalin & Karahan (1979). It is very close to the results obtained from the model of Dey (1999). The representation of the Shields parameter and the shear Reynolds number in a single curve, as was done by Shields, requires trial-and-error to solve the bed shear stress or shear velocity, as bed shear stress and shear velocity, being interchangeable, are dependent and independent variables. To avoid this difficulty, the Shields parameter is represented as a function of the particle parameter $D^*[= d_{50}(\Delta g/\nu^2)^{1/3}]$ (Dey, Dey Sarker & Debnath 1999; Dey 1999). Importantly, D^* does not involve different bed categories. However, the curve proposed by Dey (1999) for the sediment threshold can be expressed by a number of

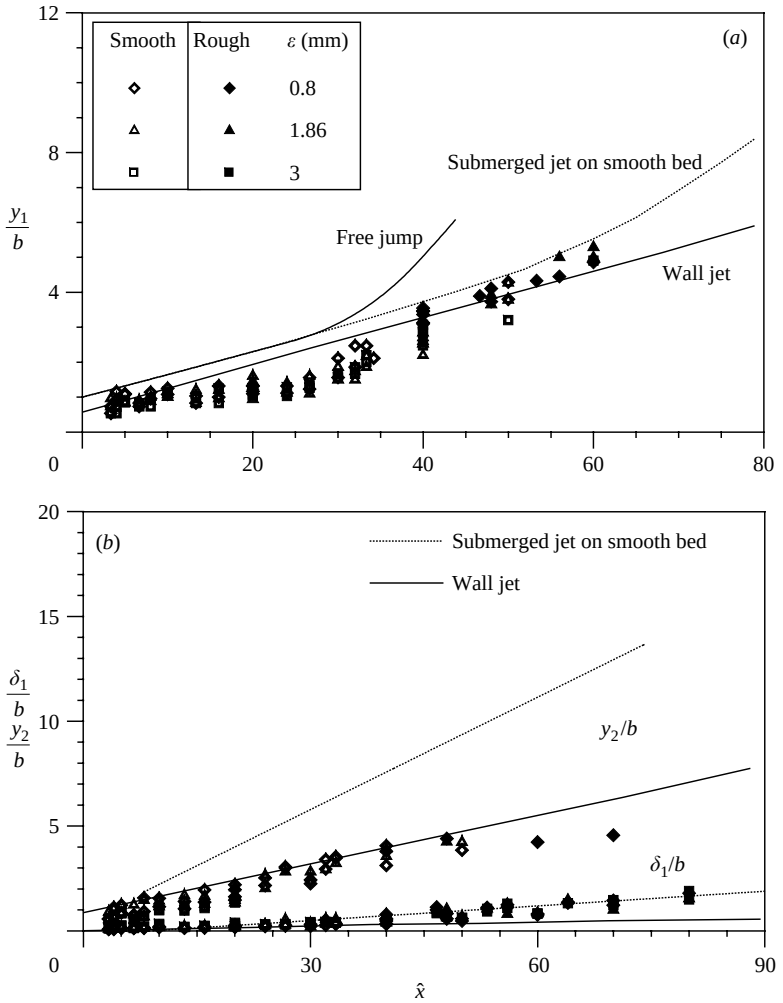

FIGURE 17. Variations of (*a*) y_1/b and (*b*) δ_1/b and y_2/b with $\hat{x}$ for different ε and $L = 0.5$ m.

simple curves as follows:

$$\Theta(D^* \leqslant 1) = 0.142/D^{*0.35}, \tag{7.2a}$$

$$\Theta(1 < D^* \leqslant 15) = 0.148/D^{*0.36}, \tag{7.2b}$$

$$\Theta(15 < D^* \leqslant 50) = 0.013D^{*0.32}, \tag{7.2c}$$

$$\Theta(D^* > 50) = 0.045, \tag{7.2d}$$

where Θ is the Shields parameter defined by $[\tau_c]_{\theta=0}/(\Delta\rho g d_{50})$, $\Delta = s - 1$ and s is the relative density of sediment. Unlike fixed rough beds, where the roughness was expressed by ε (see § 3–§ 6), it is appropriate to define the roughness of loose sediment beds by the median particle size d_{50}. For scour downstream of an apron, henceforth d_{50} is the notation for the roughness for sediment beds.

7.3. *Bed shear stress*

The bed shear stresses τ acting on the equilibrium scoured bed are estimated from the measured Reynolds stress profiles extended to the scoured bed. The non-dimensional

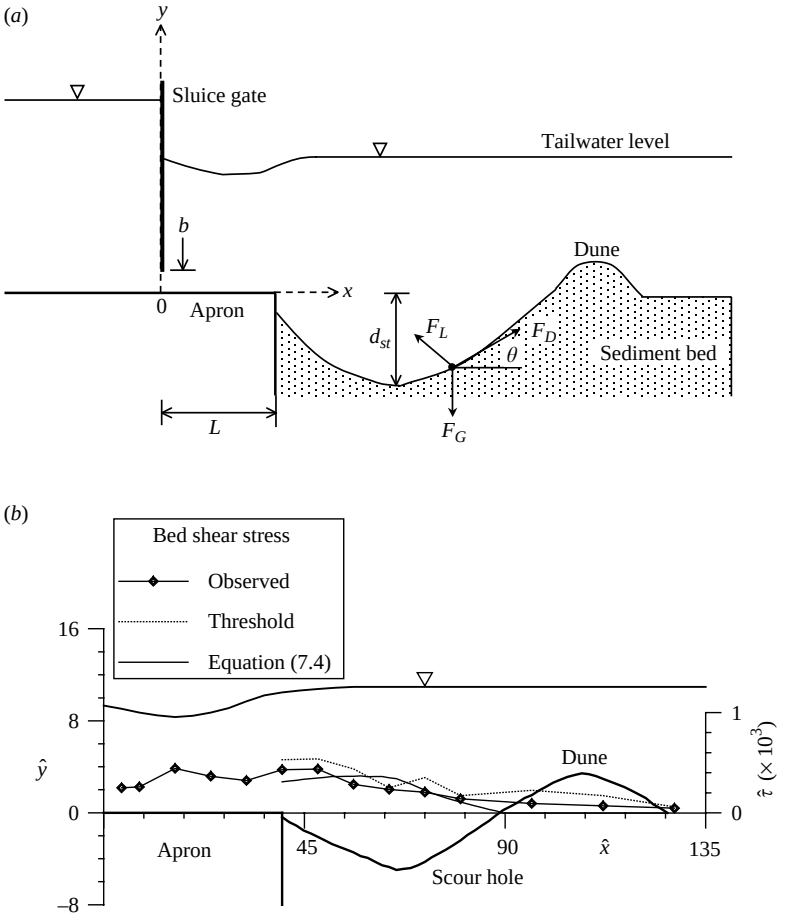

FIGURE 18. (*a*) Schematic diagram of scour downstream of an apron due to a submerged jet issuing from a sluice opening and (*b*) variations of bed shear stress $\hat{\tau}$ on scoured beds for $U = 1.435\,\mathrm{m\,s^{-1}}$, $L = 0.4\,\mathrm{m}$, $b = 12.5\,\mathrm{mm}$ and $d_{50} = 0.8\,\mathrm{mm}$.

bed shear stress $[\hat{\tau}]_{\theta=\theta}$ at any location on the scoured bed with local angle θ is given by

$$[\hat{\tau}]_{\theta=\theta} = \hat{\tau}\cos\theta. \tag{7.3}$$

In figure 18(*b*), a comparison of the experimental bed shear stress and local threshold bed shear stress, obtained from (7.1) as $[\hat{\tau}_c]_{\theta=\theta} = [\hat{\tau}_c]_{\theta=0}\cos\theta[1 + (\tan\theta/\mu)]$, shows that the surface of the equilibrium scour hole is at threshold condition. (Note: to determine $[\hat{\tau}_c]_{\theta=\theta}$ for a given d_{50}, D^* was calculated. Then, Θ was estimated from the set (7.2), and $[\hat{\tau}_c]_{\theta=0}$ from $\Theta(\Delta\rho g d_{50})$. Thus, one can calculate $[\hat{\tau}_c]_{\theta=\theta}$ as $[\tau_c]_{\theta=0}/(\rho U^2)$.) It is assumed that the bed shear stress for the two-dimensional submerged wall jet on scoured bed is equivalent to that for the two-dimensional submerged wall jet on a smooth bed followed by a rigid rough bed given by (5.1). This assumption leads to the approximation that the bed profile does not influence the self-preserving characteristics of the submerged wall jet, or alternatively, the aspect ratio of the scoured bed is small. In addition, the flow close to the bed is assumed to be not separated from the scoured bed, as was assumed by Hogg *et al.* (1997). However, this assumption may be inapt near the upstream slope of the scour hole and downstream of the dune, where the

d_{50}	c_0		c_1		c_2		c_3		c_4		
(mm)	$y \leqslant 0$	$y > 0$	$y \leqslant 0$	$y > 0$	$y \leqslant 0$	$y > 0$	$y \leqslant 0$	$y > 0$	$y \leqslant 0$	$y > 0$	n
0.8	50.4	0.91	−2.965	−0.12	0.0611	1.8×10^{-3}	-5×10^{-4}	-2×10^{-6}	1.5×10^{-6}	0	0.14
1.86	49.4	1.27	−2.965	−0.16	0.0611	2.6×10^{-3}	-5×10^{-4}	-2.8×10^{-6}	1.7×10^{-6}	0	0.15
3	50.8	1.64	−2.965	−0.2	0.0611	3.3×10^{-3}	-5×10^{-4}	-3.6×10^{-6}	1.6×10^{-6}	0	0.16

TABLE 3. Values of coefficients in equation (7.6) for different d_{50}.

flow separates. Nevertheless, it simplifies the problem considerably. Thus, one can hypothesize the bed shear stress on the equilibrium scoured bed to be

$$[\hat{\tau}]_{\theta=\theta}(\hat{x} \geqslant \hat{L}) = -\Xi(\hat{x} - \hat{L}, \hat{y}) \left[\left(2\hat{\delta}\hat{u}_0 \frac{\mathrm{d}\hat{u}_0}{\mathrm{d}\hat{x}} + \hat{u}_0^2 \frac{\mathrm{d}\hat{\delta}}{\mathrm{d}\hat{x}} \right) \int_0^\eta (\psi^2 + \phi_1 - \phi_2)\, \mathrm{d}\eta \right]. \quad (7.4)$$

The function Ξ, determined empirically using the bed shear stress obtained from the measured Reynolds stress profiles within the equilibrium scour holes, is given by

$$\Xi = 0.0081 c^{4\hat{y}/\hat{\delta}} + 0.04(c\hat{y}/\hat{\delta})^2. \quad (7.5)$$

The parameter c in the above equation, being a function of $\hat{x}$ and d_{50}, can be given by the following polynomial:

$$c = c_0 + c_1(\hat{x} - \hat{L}) + c_2(\hat{x} - \hat{L})^2 + c_3(\hat{x} - \hat{L})^3 + c_4(\hat{x} - \hat{L})^4. \quad (7.6)$$

The values of coefficients c_0, c_1, c_2, c_3 and c_4 for different d_{50} are given in table 3. Figure 18(*b*) shows that the bed shear stresses computed from (7.4), being tuned by the experimental data, compare reasonably with those determined from the Reynolds stress within the scour hole.

7.4. *Profiles of equilibrium scour hole*

The profile of the equilibrium scour hole can be computed from the threshold condition of sediment particles resting on the surface of the scour hole under the bed shear stress distribution given by (7.4). This concept has been commonly used, such as to determine the scour profiles below pipelines (Li & Cheng 1999, 2001). Using (7.1) and (7.4), the threshold condition of a sediment particle resting on the surface of the scour hole is given by

$$-\Xi(\hat{x} - \hat{L}, \hat{y}) \left[\left(2\hat{\delta}\hat{u}_0 \frac{\mathrm{d}\hat{u}_0}{\mathrm{d}\hat{x}} + \hat{u}_0^2 \frac{\mathrm{d}\hat{\delta}}{\mathrm{d}\hat{x}} \right) \int_0^\eta (\psi^2 + \phi_1 - \phi_2)\, \mathrm{d}\eta \right] \geqslant [\hat{\tau}_c]_{\theta=0} \cos\theta \left(1 + \frac{\tan\theta}{\mu} \right). \quad (7.7)$$

For the limiting equilibrium, (7.7) can be expressed as the following differential equation:

$$(\Omega^2 - 1)\frac{\mathrm{d}\hat{y}}{\mathrm{d}\hat{x}} = \mu \pm [\mu^2 - (\Omega^2 - 1)(\Omega^2 - \mu^2]^{0.5} \quad (7.8)$$

where

$$\Omega = -\frac{0.0081 c^{4\hat{y}/\hat{\delta}} + 0.04(c\hat{y}/\hat{\delta})^2}{[\hat{\tau}_c]_{\theta=0}} \left[\left(2\hat{\delta}\hat{u}_0 \frac{\mathrm{d}\hat{u}_0}{\mathrm{d}\hat{x}} + \hat{u}_0^2 \frac{\mathrm{d}\hat{\delta}}{\mathrm{d}\hat{x}} \right) \int_0^\eta (\psi^2 + \phi_1 - \phi_2)\, \mathrm{d}\eta \right]. \quad (7.9)$$

Equation (7.8) is a first-order differential equation, which can be solved numerically by the forth-order Runge–Kutta method to determine the variation of $\hat{y}$ with $\hat{x}$,

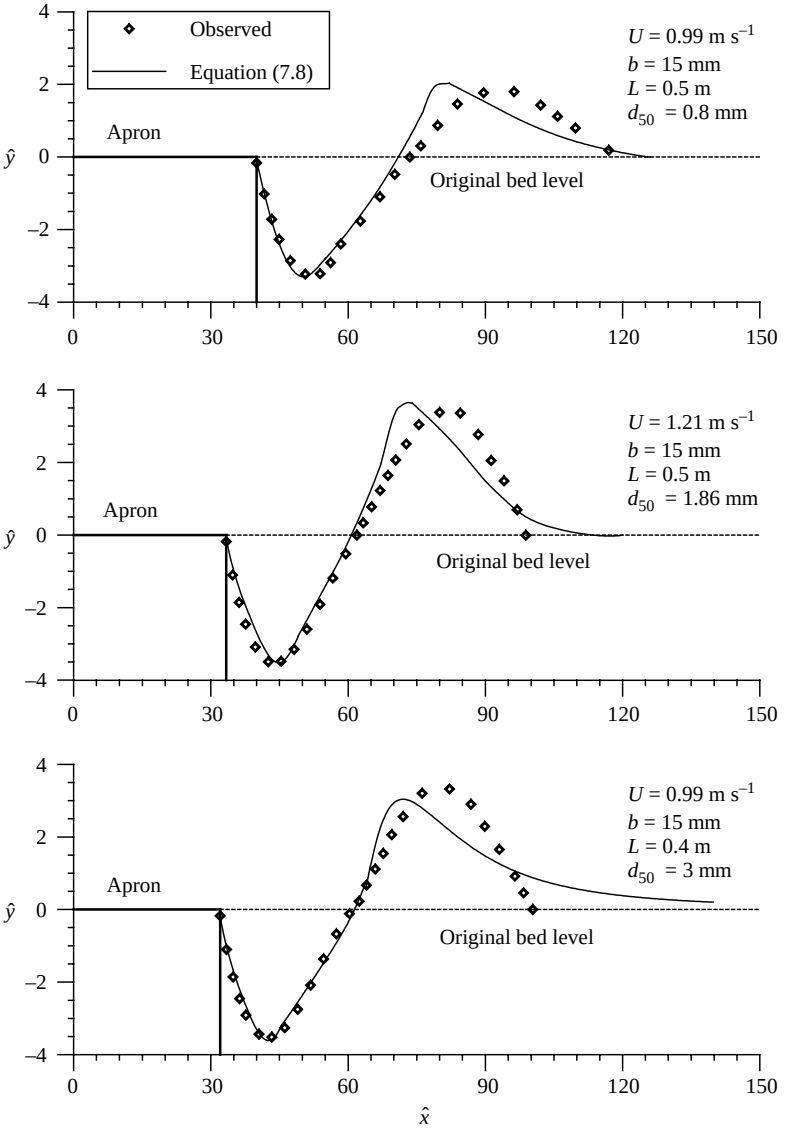

FIGURE 19. Comparisons of computed and experimental scour profiles.

that is the non-dimensional profile of an equilibrium scour hole. In (7.8) positive and negative signs are associated with the solution for scour hole ($\hat{y} \leqslant 0$) and dune ($\hat{y} > 0$) parts, respectively. In the present analysis, the value of μ was assumed to be 0.65. From the experimental profiles, it was observed that the sediments at the edge of the apron were washed away, as a result of which a small vertical portion of apron, of depth 0.35b, was exposed (Dey & Sarkar 2006). Therefore, (7.8) was solved for the initial values of $\hat{x} = \hat{L}$ and $\hat{y} = 0.35$. Figure 19 shows the non-dimensional profiles of the equilibrium scour hole. The collapse of the computed and the experimental profiles is good within the scour hole. However, over the dune, the disagreement is due to the flow separation at the crest of the dune.

7.5. *Time variation of maximum scour depth*

A simple model for the time variation of maximum scour depth (that is the maximum depression of the bed level for an instantaneous scour hole profile) downstream of an apron due to submerged wall jets is developed. It is based on the following assumptions:

(i) the bed shear stress induced by the submerged wall jets is the main agent of scouring, picking up the sediment particles from the beds;

(ii) the rate of change of sediment mass at the location (infinitesimal area) of the maximum scour depth equals the sediment mass removal rate from that location.

In a small interval of time $\mathrm{d}t$, the sediment mass picked up from the location of the maximum scour depth of small width Δx is given by

$$\mathrm{d}m_1 = \Delta x E \mathrm{d}t \tag{7.10}$$

where E is the sediment pick-up rate at the location of the maximum scour depth at time t. During scouring at the location of the maximum scour depth, estimated using the equation of van Rijn (1984), it is

$$E = 0.00033\rho_s(\Delta g d_{50})^{0.5} D^{*0.3} T^{1.5} \tag{7.11}$$

where ρ_s is the mass density of sediment and T is the transport-stage parameter due to scouring, that is $([\hat{\tau}]_0 - [\hat{\tau}_c]_{\theta=0})/[\hat{\tau}_c]_{\theta=0}$ and $[\hat{\tau}]_0$ is the bed shear stress at the location of the maximum scour depth, being time dependent. This time-dependent bed shear stress $[\hat{\tau}]_0$ can be hypothesized using an exponential function dependent on instantaneous scour depth d_{st} as follows:

$$[\hat{\tau}]_0 = -\exp[-(C_0\hat{d}_{st})^n]\left[\left(2\hat{\delta}\hat{u}_0\frac{\mathrm{d}\hat{u}_0}{\mathrm{d}\hat{x}} + \hat{u}_0^2\frac{\mathrm{d}\hat{\delta}}{\mathrm{d}\hat{x}}\right)\int_0^{\eta}(\psi^2 + \phi_1 - \phi_2)\,\mathrm{d}\eta\right] \tag{7.12}$$

where C_0 is the function of a parameter that defines the mobility of the sediment particles during scour and $\hat{d}_{st} = d_{st}/b$. Dey & Sarkar (2006) recognized that the densimetric Froude number F $(= U/(\Delta g d_{50})^{0.5})$ is the appropriate parameter which defines the mobility of the sediment particles. Here, in equilibrium profiles, the horizontal location of the maximum scour depth is approximately $\hat{x} = \hat{L} + 20$. From the comparison of the bed shear stress results on horizontal beds and equilibrium scoured beds, it is observed that the value of the bed shear stress does not vary much from $\hat{x} = \hat{L}$ to $\hat{x} = \hat{L} + 20$. Therefore, in the calculation of $[\hat{\tau}]_0$ from (7.12), $\hat{x} = \hat{L} + 10$ can be considered as an average length. Using the bed shear stresses obtained from the measured Reynolds stress profiles at the locations of the maximum scour depth of intermediate and equilibrium scour holes, the equation for C_0 and the values of n are determined empirically: $C_0 = 0.02\exp(1.09F)$; and the values of n for different d_{50} are furnished in table 3.

The depletion of sediment mass due to an increase in scour depth $\mathrm{d}d_{st}$ in time $\mathrm{d}t$ is

$$\mathrm{d}m_2 = -(1 - \rho_0)\rho_s \Delta x \mathrm{d}d_{st} \tag{7.13}$$

where ρ_0 is the porosity of the sediment. In this analysis, the value of porosity ρ_0 assumed was 0.4. From the concept of conservation of mass of sediment, the fundamental equation to describe the scouring process can be obtained as

$$\mathrm{d}m_1 + \mathrm{d}m_2 = 0. \tag{7.14}$$

Equations (7.10) and (7.13) are substituted into (7.14) to obtain the following differential equation of the time variation of maximum scour depth in non-dimensional

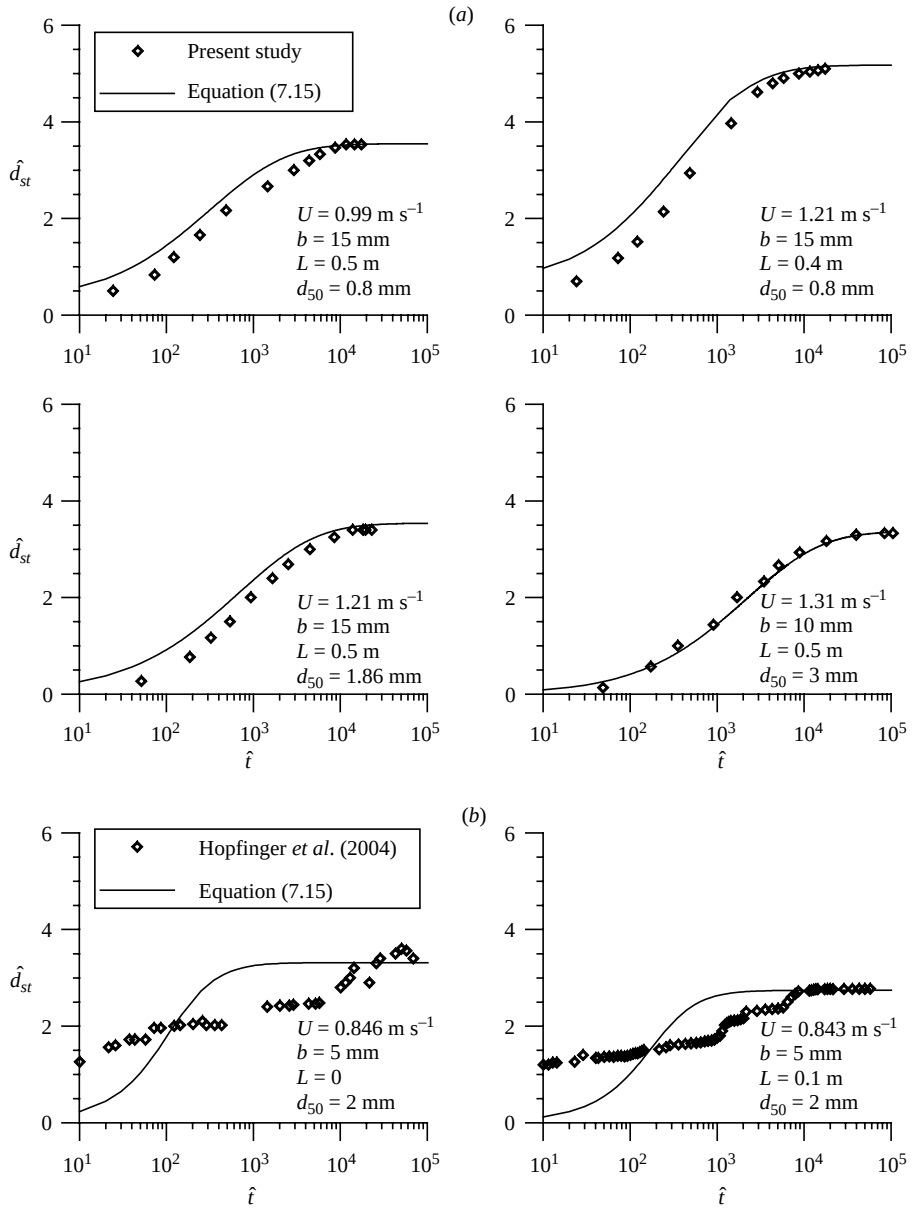

FIGURE 20. Comparisons of computed and experimental time-variation of scour depth ($\hat{d}_{st}$ versus $\hat{t}$): (*a*) data of present study and (*b*) data of Hopfinger *et al.* (2004).

form:

$$\frac{\mathrm{d}\hat{d}_{st}}{\mathrm{d}\hat{t}} = \frac{\phi_p}{(1-\rho_0)\hat{d}} \tag{7.15}$$

where $\hat{t}$ is the time parameter, that is $td_{50}(\Delta g d_{50})^{0.5}/b^2$, ϕ_p is the sediment pickup function, that is $E/[\rho_s(\Delta g d_{50})^{0.5}]$ and $\hat{d} = d_{50}/b$. Equation (7.15) is solved numerically to determine the variation of $\hat{d}_{st}$ with $\hat{t}$ for a given issuing jet velocity U, sluice opening b, apron length L and sediment size d_{50}. Figure 20 presents the curves of

non-dimensional time variation of scour depth. The collapse of the computed results and the experimental data of the present study, in figure 20(*a*), is satisfactory. However, there exists a considerable departure of the computed curves from the experimental data of Hopfinger *et al.* (2004) (figure 20*b*). Because Hopfinger *et al.* (2004) conducted the experiments either without an apron or with a short apron, where the issuing jets immediately encountered the sediment beds (while in the present study, the jet travels over an apron for a considerable distance before it encounters the sediment beds) there was a huge volume scour during the initial period, which is clearly evident from figure 20(*b*). (Note: as Hogg *et al.*'s (1997) model does not account the apron length L, it is thus applicable to the experiments of Hopfinger *et al.* (2004).) Importantly, the present model is developed for minimum length of the apron $L = 0.5(b - h_j)$, which is the minimum dimension of the apron used in practice for dissipating the energy of submerged jets. Thus, Hogg *et al.*'s (1997) model is limited in its applicability to the scour downstream of an apron, whereas the present model, which is the outcome of a fundamental study of a submerged jets on an abrupt change from smooth to rough beds, is applicable.

8. Conclusions

The flow field for the decay of jet velocity in submerged wall jets over abrupt changes from smooth to rough beds suggests that the decay rate of the jet is faster on rough beds. Hence, the growth of the boundary layer is quicker with an increase in bed roughness. The change in bed roughness induces an increased depression of the free surface over the smooth bed (figure 2). The Reynolds and bed shear stresses have been determined from the solution of the Navier–Stokes equations. The variations of flow, turbulence and stress characteristics of submerged wall jets at the junction of smooth and rough beds are gradual (figures 2–8). The response of the turbulent flow characteristics of submerged wall jets to abrupt changes from smooth to rough beds has been analysed from the point of view of similarity, growth of the length scale and decay of the velocity and turbulence characteristics scales. As there is no step change of roughness, use of a common length scale collapses the velocity and turbulence data to a single band (figures 11 and 12). The flow is mainly self-preserving on both smooth and rough beds, though in the vicinity of their junction a little data scatter exists. The decay rates of local maximum horizontal velocity component, Reynolds stress, horizontal and vertical turbulence intensity components on rough beds are faster than those on smooth beds, as a result of the mixing of fluid due to roughness (figures 11 and 12). The inner-layer thickness of the horizontal velocity component and the turbulence intensity profiles on rough beds increases with bed roughness (figures 13–16). On smooth beds, in general, the velocity and turbulence intensity distributions collapse onto the corresponding curves of submerged jets on smooth beds (figures 13*a*–16*a*). But on rough beds, they depart from the corresponding curves of submerged jets on smooth beds (figures 13*b*–16*b*). The jet half-widths on smooth and rough beds decay slower and faster than that in classical wall jets, respectively (figure 17*a*). On the other hand, the half-width of the Reynolds stresses on smooth and rough beds decays slower than those in the wall jets and submerged jets on smooth beds (figure 17*b*). However, the null-points of the Reynolds stress profiles on smooth and rough beds remain same as that in submerged jets on smooth beds (figure 17*b*).

The profiles of the equilibrium scour hole have been calculated from the threshold condition of the sediment particles along the bed surface. The modification of the bed

shear stress expression due the variation of downstream scour profile has permitted the computation of equilibrium profiles of the scour holes (figure 19). The time variation of maximum scour depth has also been estimated using the bed shear stress expression modified by an exponential function for the time dependence (figure 20). The collapse of the results obtained from the model and the present experimental data is satisfactory (figures 19 and 20).

REFERENCES

Antonia, R. A. & Luxton, R. E. 1971 The response of a turbulent boundary layer to a step change in surface roughness. Part 1. Smooth to rough. *J. Fluid Mech.* **48**, 721–761.

Chatterjee, S. S. & Ghosh, S. N. 1980 Submerged horizontal jet over erodible bed. *J. Hydr. Div. ASCE* **106**, 1765–1782.

Chen, X. & Chiew, Y. M. 2003 Response of velocity and turbulence to sudden change of bed roughness in open-channel flow. *J. Hydr. Engng ASCE* **129**, 35–43.

Dey, S. 1999 Sediment threshold. *Appl. Math. Model.* **23**, 399–417.

Dey, S. 2002 Secondary boundary layer and wall shear for fully developed flow in curved pipes. *Proc. R. Soc. Lond.* A **458**, 283–298.

Dey, S., Dey Sarker, H. K. & Debnath, K. 1999 Sediment threshold under stream flow on horizontal and sloping beds. *J. Engng Mech. ASCE* **125**, 545–553.

Dey, S. & Lambert, M. F. 2005 Reynolds stress and bed shear in nonuniform-unsteady open channel flow. *J. Hydr. Engng ASCE* **131**, 610–614.

Dey, S. & Sarkar, A. 2006 Scour downstream of an apron due to submerged horizontal jets. *J. Hydr. Engng ASCE* **132**, 246–257.

Dey, S. & Westrich, B. 2003 Hydraulics of submerged jet subject to change in cohesive bed geometry. *J. Hydr. Engng ASCE* **129**, 44–53.

Ead, S. A. & Rajaratnam, N. 2002 Plane turbulent wall jets in shallow tailwater. *J. Engng Mech. ASCE* **128**, 143–155.

Glauert, M. B. 1956 The wall jet. *J. Fluid Mech.* **1**, 625–643.

Hassan, N. M. K. N. & Narayanan, R. 1985 Local scour downstream of an apron. *J. Hydr. Engng ASCE* **111**, 1371–1385.

Hogg, A. J., Huppert, H. E. & Dade, W. B. 1997 Erosion by planar turbulent wall jets. *J. Fluid Mech.* **338**, 317–340.

Hopfinger, E. J., Kurniawan, A., Graf, W. H. & Lemmin, U. 2004 Sediment erosion by Görtler vortices: the scour-hole problem. *J. Fluid Mech.* **520**, 327–342.

Hughes, W. C. & Flack, J. E. 1984 Hydraulic jump properties over a rough bed. *J. Hydr. Engng ASCE* **110**, 1755–1771.

Li, F. & Cheng, L. 1999 Numerical model for local scour under offshore pipelines. *J. Hydr. Engng ASCE* **125**, 400–406.

Li, F. & Cheng, L. 2001 Prediction of lee-wake scouring of pipelines in currents. *J. Waterway Port Coastal Ocean Engng ASCE* **127**, 106–112.

Long, D., Steffler, P. M. & Rajaratnam, N. 1990 LDA study of flow structure in submerged hydraulic jump. *J. Hydr. Res.* **28**, 437–460.

Nezu, I. & Tominaga, A. 1994 Response of velocity and turbulence to abrupt changes from smooth to rough beds in open-channel flow. *Proc. Symposium on Fundamentals and Advancements in Hydraulic Measurements and Experimentation, Buffalo, New York*, pp. 195–204.

Rajaratnam, N. 1965 The hydraulic jump as a wall jet. *J. Hydr. Div. ASCE* **91**, 107–132.

Rajaratnam, N. 1967 Plane turbulent wall jets on rough boundaries. *Water Power* **19**, 149–153.

Rajaratnam, N. 1968 Hydraulic jumps on rough beds. *Trans. Engng Inst. Canada* **11**, 1–8.

Rajaratnam, N. 1976 *Turbulent Jets.* Elsevier.

van Rijn, L. C. 1984 Sediment pick-up function. *J. Hydr. Engng ASCE* **110**, 1494–1502.

Schofield, W. H. 1981 Turbulent shear flows over a step change in surface roughness. *Trans. ASME*: *J. Fluids Engng* **103**, 344–351.

Schwarz, W. H. & Cosart, W. P. 1961 The two-dimensional turbulent wall-jet. *J. Fluid Mech.* **10**, 481–495.

Tachie, M. F., Balachandar, R. & Bergstrom, D. J. 2004 Roughness effects on turbulent plane wall jets in an open channel. *Exps. Fluids* **37**, 281–292.

Townsend, A. A. 1956 *The Structure of Turbulent Shear Flow*. Cambridge University Press.

Townsend, A. A. 1966 The flow in a turbulent boundary layer after a change in surface roughness. *J. Fluid Mech.* **26**, 255–266.

Wu, S. & Rajaratnam, N. 1995 Free jumps, submerged jumps and wall jets. *J. Hydr. Res.* **33**, 197–212.

Yalin, M. S. & Karahan, E. 1979 Inception of sediment transport. *J. Hydr. Div. ASCE* **105**, 1433–1443.